Tissue Eng Regen Med
https://doi.org/10.1007/s13770-023-00599-w

Online ISSN 2212-5469

ORIGINAL ARTICLE

Understanding the Multi-Functional Role of TCTP in the Regeneration Process of Earthworm, *Perionyx excavatus*

Kamarajan Rajagopalan[1] · Jackson Durairaj Selvan Christyraj[1] · Karthikeyan Subbiahanadar Chelladurai[1,2] · Puja Das[1] · Karthikeyan Mahendran[3] · Logeshwari Nagarajan[1] · Saritha Gunalan[1]

Received: 6 April 2023 / Revised: 30 August 2023 / Accepted: 18 September 2023
© Korean Tissue Engineering and Regenerative Medicine Society 2023

Abstract

BACKGROUND: Regeneration is a highly complex process that requires the coordination of numerous molecular events, and identifying the key ruler that governs is important to investigate. While it has been shown that TCTP is a multi-functional protein that regulates cell proliferation, differentiation, apoptosis, anti-apoptosis, stem cell maintenance, and immune responses, but only a few studies associated to regeneration have been reported. To investigate the multi-functional role of TCTP in regeneration, the earthworm *Perionyx excavatus* was chosen.

METHODS: Through pharmacological suppression of TCTP, amputation, histology, molecular docking, and western blotting, the multi-function role of TCTP involved in regeneration is revealed.

RESULTS: Amputational studies show that *P. excavatus* is a clitellum-independent regenerating earthworm resulting in two functional worms upon amputation. Arresting cell cycle at the G1/S boundary using 2 mM Thymidine confirms that *P. excavatus* execute both epimorphosis and morphallaxis regeneration mode. The pharmacological suppression of TCTP using buclizine results in regeneration suppression. Following the combinatorial injection of 2 mM Thymidine and buclizine, the earthworm regeneration is completely blocked, which suggests a critical functional role of TCTP in morphallaxis. The pharmacological inhibition of TCTP also suppresses the key proteins involved in regeneration: Wnt3a (stem cell marker), PCNA (cell proliferation) and YAP1 (Hippo signalling) but augments the expression of cellular stress protein p53.

CONCLUSION: The collective results indicate that TCTP synchronously is involved in the process of stem cell activation, cell proliferation, morphallaxis, and organ development in the regeneration event.

Keywords TCTP · Buclizine · Wnt3a · p53 · Hippo signaling

1 Introduction

The homeostatic process known as 'regeneration' directs the recovery of damaged or lost tissues [1]. Generally, epimorphosis and morphallaxis are the main principles of regeneration [2–4]. There are differences and similarities between the two processes. After wound induction, the primary tissue injury response invites stem cells from the niche [5, 6] and will accumulate at the wound site that depends on signals for healing and regeneration [7]. The cellular mechanism of apoptosis [8] and immune responses are essential for the morphallaxis mode of regeneration,

✉ Jackson Durairaj Selvan Christyraj
jacksondurairaj@sathyabama.ac.in;
jacksondurairajs@gmail.com

[1] Molecular Biology and Stem Cell Research Lab, Centre for Molecular and Nanomedical Sciences, International Research Centre, Sathyabama Institute of Science and Technology (Deemed to be University), Chennai, Tamilnadu, India

[2] School of Health Sciences, Purdue University, 550 Stadium Mall Drive, West Lafayette, IN 47907, USA

[3] Department of Zoology and Microbiology, Thiyagarajar College, Madurai, Tamilnadu, India

Published online: 07 November 2023

and tissue-specific stem cells are not required in this process [9] But epimorphosis requires tissue-specific stem cells, apoptosis, and immune responses [10, 11]. For example, *Hydra vulgaris* follows only morphallaxis [12], limb regeneration of *Xenopus laevis* froglet follows the epimorphosis mode of regeneration [13], and planarians follow both the regeneration principles [8]. Earthworms like *Eudrilus eugeniae* and *Perionyx excavatus* can regenerate their tails, segments, or even entire bodies from fragments that break off from the original worm. The pieces need a portion of the digestive and reproductive systems for regeneration. Earthworms can also regenerate lost tissue through the growth of new cells. This type of regeneration is more limited than fragmentation regeneration and can occur when the earthworm has minor injuries or is damaged but not fragmented [6].

During restoration, the earthworm's body undergoes several cellular and molecular changes. The regeneration process begins with forming a blastema, a group of undifferentiated cells that can differentiate into the specific cell types required to regenerate the lost body part. The blastema grows and differentiates into the tissues needed for the new body part, such as muscles, nerves, and skin. Apoptosis is critical in regenerating body parts in *E. eugeniae* and other earthworms and maintaining tissue homeostasis in these organisms [14]. During the regeneration process, apoptotic cells help break down and remove damaged tissue, stimulating the proliferation of new cells in the blastema. In addition to its role in tissue remodeling during regeneration, apoptosis also plays a role in maintaining tissue homeostasis in earthworms. Studies have shown apoptotic cells in the reproductive organs of earthworms during spermatogenesis, where they help remove excess cells and maintain the proper balance of germ cells and support cells [15].

When cells die because of stress or damage, it can cause the remaining cells to divide more, a process termed "apoptosis-induced compensatory proliferation (AICP)." Stem cells must proliferate and differentiate for the compensation, but this whole process depends on various signaling molecules, such as Wnt and Hh, produced from apoptotic caspases in response to cell damage [16–19]. Apoptotic executioner caspases proceed with Apoptosis Induced Apoptosis (AIA) and AICP to compensate for lost parts [20, 21]. Those driving caspases may belong to Feeder cells [22, 23]. Collective reports indicate that most of the animal models such as *Hydra*, planarians, newts, *Drosophila melanogaster*, and mouse follow AICP for the reformation of lost parts [16, 24–28]. In earthworms, apoptotic cells were observed throughout their cell renewal period of regeneration [14]. On another side, in juvenile *E. eugeniae* worms, the movement of stem cells from the clitellum to the wound site was observed [5]. However, the connective link between apoptosis and stem cells is still unclear.

According to the recent report of transcriptomic analysis of *E. eugeniae*, while more than 3986 genes are upregulated during their regeneration [29], silencing a single protein called Translationally Controlled Tumor Protein (TCTP) influences the entire progress of regeneration of *E. eugeniae* regeneration [30]. TCTP has both apoptotic and anti-apoptotic functions [31, 32] and can decide the fate of cells [33]. TCTP also plays a remarkable role in regeneration [30] and regulates major cellular mechanisms like proliferation, cell homeostasis, and survival [34], maintaining the stability of p53 [32]. For example, reciprocal repression between TCTP and p53 was observed in knockout mice models [35].

Researchers have used chemicals and siRNAs for silencing TCTP, such as Buclizine and Nutlin-3a [30]. Seo and Efferth [43] confirmed that buclizine could block the TCTP protein in MCF-7 cell lines at the cellular level. The tropical earthworm, *Perionyx excavatus*, has a unique regeneration ability [36]. The survival capacity of *P. excavatus* is higher than other earthworm species [37]. *P. excavatus* is a regeneration animal model for the central nervous system and tissue regeneration [37, 38]. Within two weeks of the amputation, *P. excavatus* achieves complete regeneration, including rebuilding vital organs [37]. Recently, Bae et al. [37] observed the epimorphosis mode of head regeneration in the earthworm *P.* excavatus [37], but the role of morphallaxis in earthworms is vague. Martinez et al. [39] suggest that the earthworm might follow both epimorphosis and morphallaxis regeneration patterns due to high predatory injury, but clear scientific evidence is unclear [40].

We observed that *P. excavatus* follows both epimorphosis and morphallaxis forms of regeneration in the present study. In addition, we report that TCTP governs morphallaxis along with the epimorphosis pattern of regeneration. Also, we provide direct evidence that TCTP is a multi-functional protein that regulates many functions associated with the regeneration mechanism, especially in association with AICP.

2 Materials and methods

2.1 Earthworm rearing and maintenance

We reared the Earthworm, *Perionyx excavatus*, from the stock maintained in the Centre for Molecular and Nanomedical Sciences, International Research Centre, Sathyabama Institute of Science and Technology, Chennai, Tamilnadu, India. Earthworms were maintained according to the standard protocol [39–42]. Cow dung and leaf litter

were fed to worms in equal amounts and kept in the plastic tub at the appropriate moisture condition.

2.2 Cell cycle arresting assay

To block epimorphosis, 2 mM thymidine was injected into the 24th segment of the worms (No: 10). Nuclease-free water injection was used for the control set of worms (No: 10). An injection was continued for up to 10 days. After the second day of injection, the worms were amputated on the 10th segment and observed for their regeneration kinetics with a 15 cm scale and camera.

2.3 Buclizine injection and pharmacological suppression of TCTP

In this experiment, three dose levels of Buclizine (Mankind Pharma Ltd, Chennai, India), namely 140 μg, 160 μg, and 200 μg, were injected into the post-clitellum regions (24th segment) of *P. excavatus* worms once per day throughout the experiments. The control worm was injected with 1X PBS. Following 2nd day of the initial injection, the worms were amputated at the 10th segment and observed for regeneration ability. The regeneration process was monitored and documented using a Canon digital camera (IXUS 285 HS).

2.4 Regeneration studies

We used the eight groups of mature *P. excavatus* worms in this study to understand the importance of TCTP in regeneration. Each group consisted of ten worms, and the treatment is as follows: 1. *in vivo* regeneration analysis, 2 and 3. Control and Buclizine treatment for TCTP silencing, 4 and 5. Control and Thymidine treatment for cell arrest analysis, and 6. Buclizine and thymidine treatment for combinatorial toxicology. 7 and 8. Control and Nutlin-3a treatment for TCTP silencing. For *in vivo* regeneration analysis, selected worms (group 1) were amputated in the 10th segment (anterior region-head) using a cruzine carbon steel surgical scalpel blade (size 15) and maintained in the worm bed. Every 24 h, the amputated worms were documented with the help of a canon digital camera (IXUS 285 HS).

2.5 Influence of Nutlin-3a in regeneration

To study the importance of TCTP in regeneration, mature *P. excavatus* worms were selected. Two batches were selected, each containing 10 worms, 10 for control and another 10 for Nutlin-3a treatment. The first batch of ten worms acted as a control and was injected with DMSO. The second batch of ten worms was injected with Nutlin-3a in the 24th segment at a dose of 5 μg/g. The control and treated worms were amputated at the 10th segment (anterior) and maintained in the soil. The worms were anesthetized by ice before amputation. The blastemal formation was carefully observed in both batches of worms with the help of a Canon digital camera (IXUS 285 HS).

2.6 Histology

Thymidine-treated 7th day regenerated worms, 5th day Nutlin-3a treated samples and their respective control samples were subjected to histological sectioning. Both the regeneration blastema of the control and treated worms were cut using sterile scalpels along with the adjacent two segments and fixed in 10% formaldehyde (Cat.F0080; Rankem, Mumbai, India) for 24 h. To remove formaldehyde, tissues were gently washed with distilled water and dehydrated with isopropanol and acetone after the tissue was cleared using xylene. Each step was performed for one hour at 50 °C. Following the xylene removal step, tissue impregnation was incubated in paraffin wax, and the 5 μm sections were made using a microtome [30]. Eosin and hematoxylin stains were used to distinguish the internal arrangements and were observed in Euromex bScope Epi-Fluorescence HBO Microscope (Catalogue Number: BS.3153-PLFi).

2.7 Western blotting

All experiment samples were quantified using Lowry's method, and an equal volume (80 μg) of protein samples was loaded onto SDS page gel electrophoresis and applied to run at 60 volts for 2 h 30 min using Bio-Rad gel systems. The resolved proteins in the SDS-PAGE gel were transferred to the PVDF membrane. The membrane was blocked with 5% BSA in TBST buffer and then incubated with either of the following primary antibodies of Anti-TCTP (Abcam [Cambridge, UK], ab37506; dilution, 2.5:5000), Anti-p53 (Abcam, ab26; dilution, 2.5:5000) and Anti-β-actin (Abcam, ab8226; dilution, 1:5000), Anti-Wnt3a (Abcam, ab19925; dilution, 0.5:5000), Anti-PCNA (Abcam, ab18197), Anti-H3 (Abcam, ab1791; dilution, 1:5000) and Anti-YAP1 (Abcam, ab62751; dilution, 0.5:5000) for overnight at 4 °C. After washing, the secondary antibody of Anti-rabbit IgG-HRP (1:10000) or Anti-mouse IgG-HRP (1:10000) was added to protein transferred membrane. The substrate ECL was used as a developer solution. ChemiDoc XRS documented the developed membrane, Bio-Rad (Hercules, CA, USA); the band intensity was analyzed using ImageJ analysis software (NIH, Bethesda, MD, USA).

2.8 Homology modelling of TCTP protein

TCTP of *Lumbricus rubellus* (Humus earthworm) was selected as the target sequence for the study. The one-dimensional FASTA sequence of the target protein, TCTP, were retrieved from the UniProt protein sequence database with accession number 018477. The structural blast was performed with the TCTP sequence of *L. rubellus* against the PDB database to identify the template structure for homology modelling. The homology model of *L. rubellus* TCTP protein was generated by SWISS-MODEL homology modelling server with the crystal structure of human histamine releasing factor-translationally controlled tumor protein (HRF-TCTP) (PDB ID: 5O9M) as the template structure. The quality and reliability of the constructed model were evaluated by PROCHECK, ERRAT, and VERIFY3D servers.

2.9 Ligand preparation for docking

The structure of the ligand, buclizine, was constructed using the 2D/3D ChemBio Draw Ultra software application, version 12 (Cambridge Soft, Cambridge, MA, USA), and then copied into the ChemBio 3D Ultra software application, version 12, to create the 3D structure. Then the structure was energy minimized by the MMFF94 method using the geometry optimization function in Chem Draw 3D software, and the lower energy conformations were selected for molecular docking studies.

2.10 Molecular docking studies

A molecular docking process was carried out using Autodock vina to reveal the binding analysis of *L. rubellus* (closely related species of *P. excavatus*) TCTP protein vs. Buclizine (PubChem ID: 6729). The protein's binding site was adjusted using a grid box and x, y, and z-axis values. The grid box (60ÅX 60Å X60Å) is centered at 4.066, 20.626, − 11.479, and the spacing is 1. All other parameters were kept as default. An exhaustiveness of 10 was assigned for docking throughout the docking process, and 10 mode numbers were assigned to achieve reliable results. Post-docking analyses were carried out using Discovery Studio.

3 RESULTS

3.1 Anterior regeneration and tissue growth in the earthworm, *P. excavatus*

The earthworm *P. excavatus* is a bright brown segmented worm, and its clitellum segments are located between 13 to 17th segments, as shown in Fig. 1A. The worms were amputated at the 50th segment, i.e., away from the clitellum segments, and observed for their regeneration ability. The amputated anterior segments with head and clitellum can regenerate the tail on the 8th day of post-amputation. Similarly, the other portion of amputated posterior segments without clitellum segments form the regenerative head on the 8th day of post-amputation, as shown in the Fig. 1B. To understand the wound healing and regenerative dynamics of anterior regeneration, the earthworms are amputated at the 10th segments and observed every 24 h, as shown in Fig. 1C–G. Following 24 h of post-amputation, perfect sealing of amputation sites occurs with the formation of deep furrow (Fig. 1C), and wound healing was distinctly observed following 48 h of post-amputation (Fig. 1D). The worm starts to restore their lost tissue by forming a pre-blastemal structure following 72 h of post-amputation (Fig. 1E) and with increased size in 96 h (Fig. 1F). In proceeding days, the blastema starts to elongate further and differentiate to form the new lost segments following 120 h of post-amputation as shown in Fig. 1G.

3.2 *P. excavatus* follows both epimorphosis and morphallaxis patterns for their regeneration

To further investigate the regeneration mechanism of clitellum-independent *P. excavatus* worm, the worms were injected with 2mM Thymidine to arrest the cell proliferation or synchronize the cells in the G1/S phase. The worms injected with 2mM Thymidine as described in materials and method are amputated on the 2nd day and observed for regeneration ability on the 2nd, 4th, 6th, and 8th day of post-amputation (Fig. 2A–H). The result shows that in the control worm, the blastema starts to project out on the 2nd day of post-amputation, but in the 2mM thymidine-injected worm, it is visible only with wound healing. On successive days of the 4th, 6th, and 8th days of post-amputation, the size of the regenerative bud is 1/3rd reduced in 2mM Thymidine injected worm when compared with the control worms. The delayed regeneration following cell proliferation inhibition with 2mM thymidine injection represents the worms following morphallaxis and epimorphosis for their regeneration. Comparative histological analysis of the 8th day of the regenerative bud of control and 2 mM thymidine-treated worms shows that in control worms, the bud segments are well elongated along with septum formation however this was not observed in Thymidine treated groups (Fig. 2I, J). Also, in the control worm, the functional mouth is formed along with a well-developed prostomium, but in 2 mM thymidine-treated worms, it initiates the formation of the intestine without forming a functional mouth and prostomium (Fig. 2I, J).

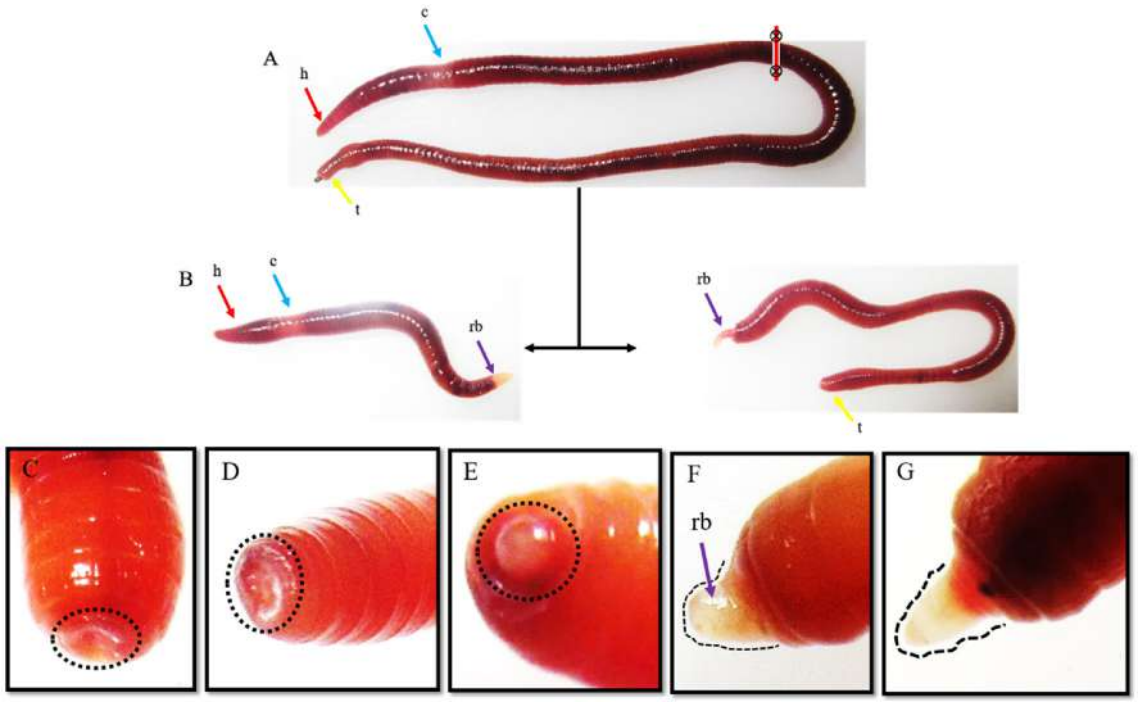

Fig. 1 Regeneration dynamics in clitellum independent earthworm, *P. excavatus*: **A** The earthworm, *P. excavatus*, appears red-brown and possesses an anterior head followed by clitellum, intestine, and anus. **B** amputation of earthworm at post-clitellum segments (50th segments), resulting in the development of two individual worms following eight days of post-amputation. **C** Following 24 h of post-amputation at the 10th segment, the wound sites were sealed by the contraction of surrounding tissues. **D** proliferative cells fill the deep furrow following 48 h of post-amputation **E** Pre-blastema structure was visibly observed on 72 h of post-amputation **F** Blastemal size elongated following 96 h post-amputation **G** Elongated blastema starts to differentiate and form visible segments following 120 h of post-amputation

3.3 Pharmacological suppression of TCTP using Buclizine, modelling of TCTP protein, and molecular docking of TCTP and Buclizine

Buclizine is an antihistamine and anticholinergic compound used to prevent the symptoms caused by histamine activity. Buclizine has effectively inhibited the TCTP protein in human cells [43]. Buclizine was injected into the worm in different concentrations of 140 µg, 160 and 200 µg and observed for the regeneration ability to identify the role of TCTP in *P. excavatus* regeneration, as shown in Fig. 3A, L. The results show that different buclizine concentrations hinder regeneration on the 1st, 4th, and 6th day of post-amputated worms to a level of 1/4th compared to the control worms. Also, we observed no significant difference among the different concentrations of buclizine used in these experiments. Therefore, we preferred a lower concentration of 140 µg for further Western blotting investigations. Protein samples are prepared from 3rd and 5th-day control regenerating and buclizine-injected regenerated worms and subjected to Western blotting against TCTP (19 kDa) and β-actin proteins (Fig. 3M). The results indicate that in control regenerating worms, TCTP upregulated in succeeding days of the 3rd and 5th days of post-amputation. On the other hand, in the buclizine-treated worms, TCTP is completely inhibited on 3rd day of buclizine-injected regenerated worms but negligibly observed on 5th day. The β-actin is used as a positive control, and its molecular weight is 42 kDa. The graphic representation of normalized values is shown in Fig. 3N.

We performed homology modelling by generating a *L. rubellus* TCTP 3D protein structure. Human histamine-releasing factor-translationally controlled tumor protein (HRF-TCTP) (PDB ID: 5O9M) was selected as the template structure for protein model building. The template 5O9M exhibited 47.90% sequence identity and a GMQE score of 0.71 with *L. rubellus* TCTP protein. The above parameters confirm that the template 5O9M could be the best template for homology modelling. The PROCHECK server evaluated the stereochemical quality of the protein model. The results of the PROCHECK server (Fig. 3O) confirmed that 93.2% of residues were in the most favored regions, and none were placed in disallowed areas. The above result confirms that the generated 3D structure of *L. rubellus* is a reliable and good-quality model. In addition to the stereo-chemical assessment, the local errors of unbounded atomic interactions were assessed by the ERRAT server (Fig. 3P). The ERRAT analysis showed an

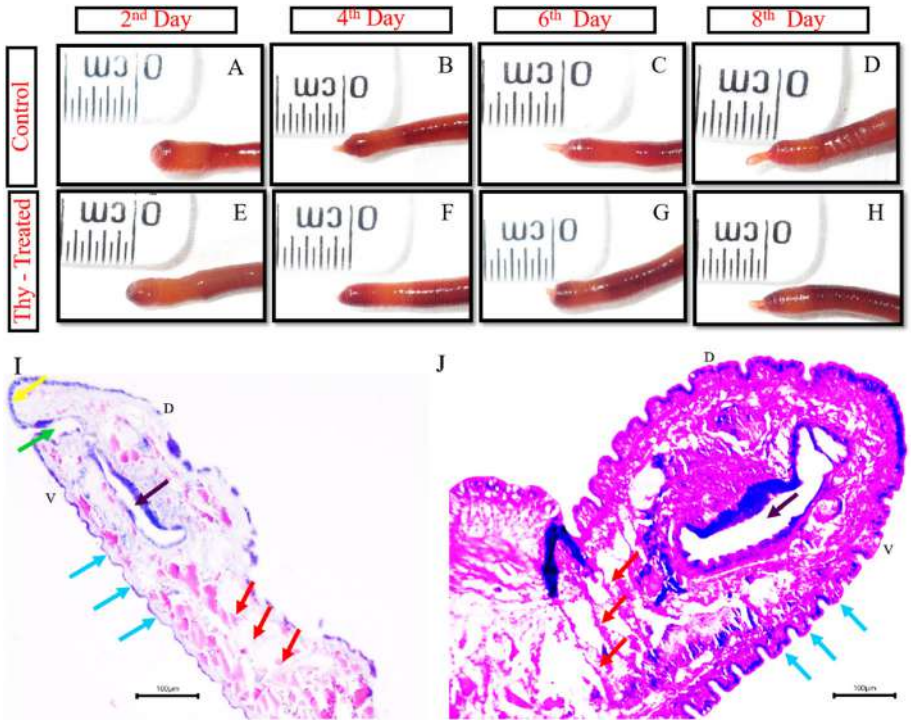

Fig. 2 Regeneration following 2 mM Thymidine (cell cycle inhibitor) injection: **A** Control worm heals wound on 2nd day of post-amputation. **B** Blastema size of 0.2 mm was observed on the 4th day after post-amputation. **C** regenerative bud elongated to 0.3 mm on the 6th day. **D** blastemal size almost doubled (0.5 mm) on the 8th day upon restoration. (E) wound healing was adequately executed in Thymidine treated worm on the 2nd day of post-amputation. **F** blastemal growth is restricted and shows only 0.1 mm size following the 4th day of post-amputation. **G** unmeasurable very little blastemal growth progress was observed until the 6th day of post-amputation. **H** blastemal size is slightly elongated to 0.2 mm size following the 8th day of post-amputation. **I** histology of 8th day control blastemal tissue shows well-differentiated prostomium, mouth, septum, and elongated segments. **J** histology of 2 mM Thymidine injected 8th day regenerative blastema with less developed structures lacking prostomium, mouth, and with truncated regenerative body segments. Arrows (red represents septum; blue represents newly regenerated segments; yellow indicates prostomium; green represents functional mouth; purple represents intestinal tract). "D" represents the dorsal side of the earthworm, and "V" specifies the ventral surface of the earthworm

overall quality factor of 98.5% for the homology-modelled 3D structure of *L. rubellus*. Further, the compatibility of the 3D atomic model of *L. rubellus*, TCTP protein with its 1D sequence was assessed by VERIFY 3D server. It is evident from the result that 99.40% of the residues with an average 3D-1D score were achieved. Therefore, all the above results confirmed the modelled 3D structure of *L. rubellus* TCTP protein as the quality model for further theoretical studies.

According to molecular docking results, buclizine formed hydrogen bonding and hydrophobic interactions with *L. rubellus* TCTP protein with a binding energy of − 6.1 kcal/mol. Two hydrogen bonds were interacting with the TCTP residues ASN49 and ALA 45 with a bond length of 3.6 Å and 3.5 Å (Fig. 3Q). Hydrophobic interactions were displayed with four residues: ALA 50, ILE 41, ALA 62, and ALA 45, as shown in Table 1. A notable feature in the docking analysis was that the residue ALA 45 exhibited hydrogen bonding and non-bonded interactions towards the ligand buclizine. The above results suggest that the residue ALA 45 and the adjacent flanking residues are the active site region of *L. rubellus* TCTP protein.

3.4 TCTP and its role in morphallaxis following combinatorial injection of buclizine and thymidine

P. excavatus regenerates through epimorphosis (cellular proliferation) and morphallaxis (trans-differentiation), as confirmed by 2 mM thymidine injection. There is currently no report available in the academic literature that comprehensively covers the morphallaxis mechanism, specifically concerning trans-differentiation, within the context of TCTP. We administered a combination of 2mM Thymidine (an epimorphosis blocker) and Buclizine (a TCTP suppressor) to investigate the matter and show the results in Fig. 4A–I. Well-differentiated blastema was observed in the control group of worms on the 8th day, as depicted in

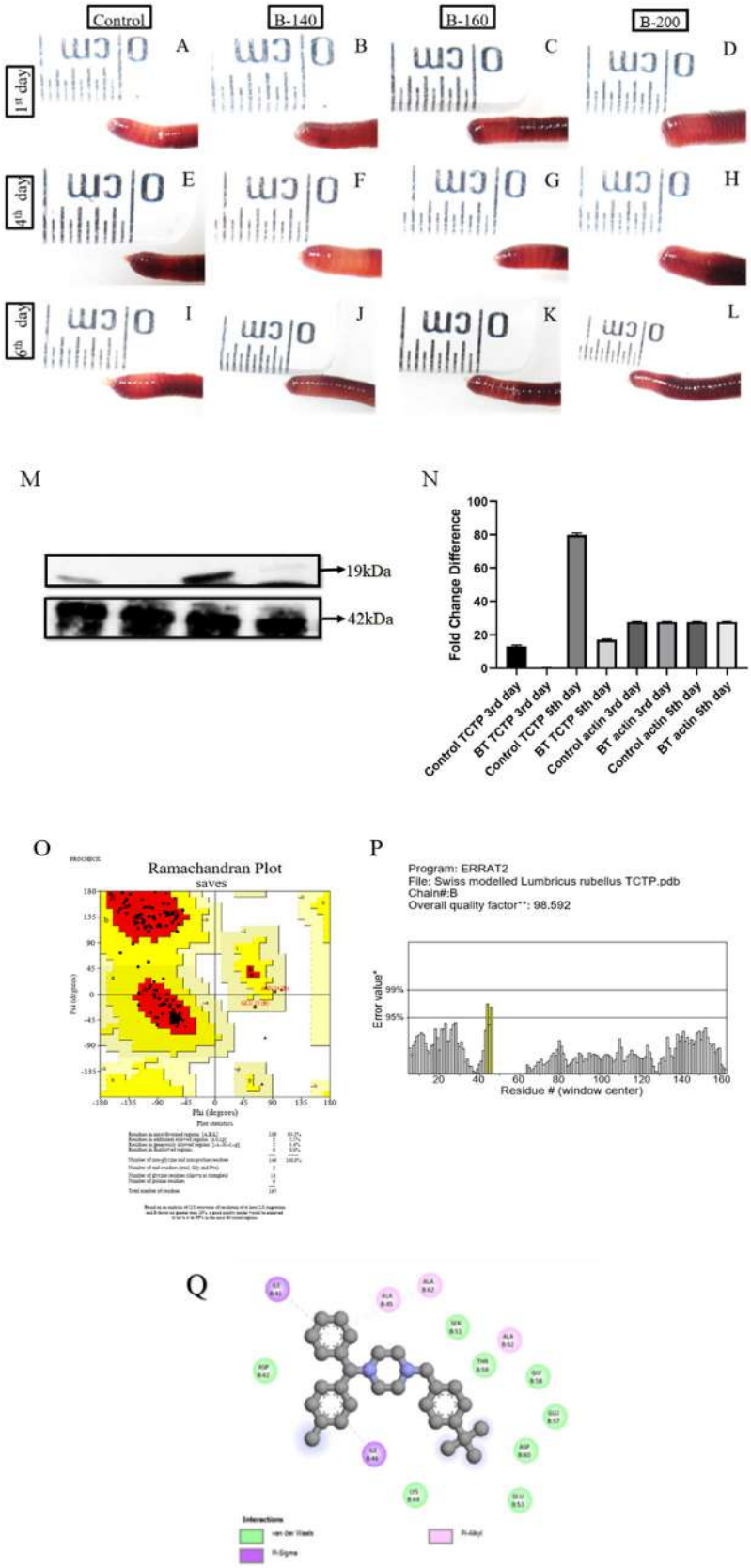

Fig. 3 Pharmacological suppression of TCTP using buclizine and its effects on regeneration: **A–D** represents control worm (1X PBS), 140 µg buclizine, 160 µg buclizine, and 200 µg buclizine injected worms respectively following day-1 of post-amputation. **E–H** represents the 4th day post amputated worms correspondingly from the control worm (1X PBS), 140 µg buclizine, 160 µg buclizine, and 200 µg buclizine injected worms. In all the buclizine-injected worms, the regenerative bud size is hindered. Similarly, **I-L** represents the 6th day regenerative bud from the control worm, 140 µg buclizine, 160 µg buclizine, and 200 µg buclizine-injected worms, respectively. In all the buclizine-injected worms, regeneration is 1/4th reduced. M. Western blotting image represents TCTP (19 kDa) and β-actin (42 kDa) expression in 3rd day control regenerating worm, 3rd day buclizine injected regenerating worm, 5th day control regenerating worm and in 5th day buclizine injected regenerating worms respectively. N. graphical representation of Western blotting results shows the fold difference of TCTP and the expression of β-actin in control regenerating worms and the 5th day buclizine injected regenerating worms. O. Stereo chemical validation of predicted *L. rubellus* TCTP protein using Ramachandran plot. P. Evaluation of *L. rubellus* TCTP protein for unbounded atomic interactions by ERRAT server. Q. *In-silico* prediction of molecular-level interaction between Buclizine and TCTP protein

Table 1 *In-silico* docking analysis of TCTP versus Buclizine

S. no	Protein	Ligand	Affinity	RMSD (I. B.)	RMSB (U. B.)	No. of bonds	Peptide– llele interaction (non-bound)	Distances	Category
1	TCTP (*Lumbricus terrestris*)	Buclizine	− 6.1	4.633	8.898	2 hydrogen bonds	:UNK0:C - B:ASN49:O	3.64063	Hydrogen Bond
						+	:UNK0:C - B:ALA45:O	3.58072	Hydrogen Bond
						6 hydrophobic bonds	B:ALA50:CB - :UNK0	3.9661	Hydrophobic
							:UNK0:Cl - B:ILE41	5.40736	Hydrophobic
							:UNK0:Cl - B:ALA62	4.17849	Hydrophobic
							:UNK0:C - B:ALA50	4.28267	Hydrophobic
							:UNK0 - B:ALA45	4.19758	Hydrophobic
							:UNK0 - B:ALA45	4.92024	Hydrophobic

Fig. 4A–C. The combinational injection of Buclizine and Thymidine completely inhibited the regeneration process for eight days post-amputation (Fig. 4D–F). However, there were no observable adverse effects on the physiological survival of the worm. The findings above suggest that TCTP governs cellular proliferation (epimorphosis) and substantially influences the morphallaxis (trans-differentiation) mechanism of regeneration, as evidenced by the total hindrance of regeneration. When we injected the worms with a double dose (two doses per day) of either 2 mM Thymidine or Buclizine, their physiological functions shut down, leading to their death within 6 days. The Mantel-Cox test was utilized to calculate and present the survival rate of worms treated with a double dose of Buclizine and Thymidine, as illustrated in Fig. 4G. The study revealed a reciprocal repression of the TCTP/p53 pattern in samples treated with buclizine/thymidine, as evidenced by the significant upregulation of p53 expression in TCTP-blocked samples (Fig. 4H–I).

3.5 Inhibition of TCTP through Nutlin-3a and their counter effect on essential regenerative proteins

Nutlin-3a indirectly promotes TCTP degradation by activating p53. To further understand the function of TCTP in regulating the key regenerative proteins, the TCTP is pharmacologically inhibited using Nutlin-3a in three different dosages of 5, 7, and 9 µg injection. When compared with the control worms, the Nutlin-3a injected worms show an overall reduced bud size (5th day) in all the concentrations (Fig. 5A [I–IV]). It is also evident that increasing the level of Nutlin-3a gradually hinders the regeneration process in the earthworm *P. excavatus.* For further histological and western blotting experiments, Nutlin-3a (9 µg) injected worm samples were taken for analysis. Comparative histology of the regenerative bud tip between control (Fig. 5B) and 9 µg Nutlin-3a injected worms (Fig. 5C) shows that the outermost epithelial layer is well organized and thicker in control worm but which is lacking in Nutlin-3a treated worms. Also, the next inner layer, the outer epithelial layer, has a thickened outer covering in the control worm, which is more thinned in treated worms. The bud interior shows more compact structures in control worms but is highly diffused without any organized form observed in Nutlin-3a treated worms. Collectively, Nutlin-3a confirms that it had a direct influence on cell package and implies the role of TCTP in holding all-essential cellular functions towards regeneration. To confirm further Western blotting was performed in control and Nutlin-3a treated worms against PCNA (cell proliferation), Wnt3a (stem cell marker), and YAP1 (organ formation ruler and Hippo signaling). The results revealed that TCTP influences all the critical regeneration proteins upon inhibiting with Nutlin-3a (Fig. 5D). PCNA, Wnt3a, and YAP1 are remarkably reduced in all TCTP-inhibited worms, and it is evident that TCTP is a multi-functional protein that governs many functions associated with the regeneration mechanism. The graphical representation of the influence of Nutlin-3a in inhibiting TCTP and its associated proteins in regeneration have shown in Fig. 5E.

4 Discussion

P. excavatus is a topsoil earthworm that is habitually subjected to injury by predators, and correlating it with its enormous posterior regeneration ability represents its evolution nature to survey following an injury [36]. Regeneration studies show that the earthworm, *P. excavatus*, has an enormous regeneration ability. The worms

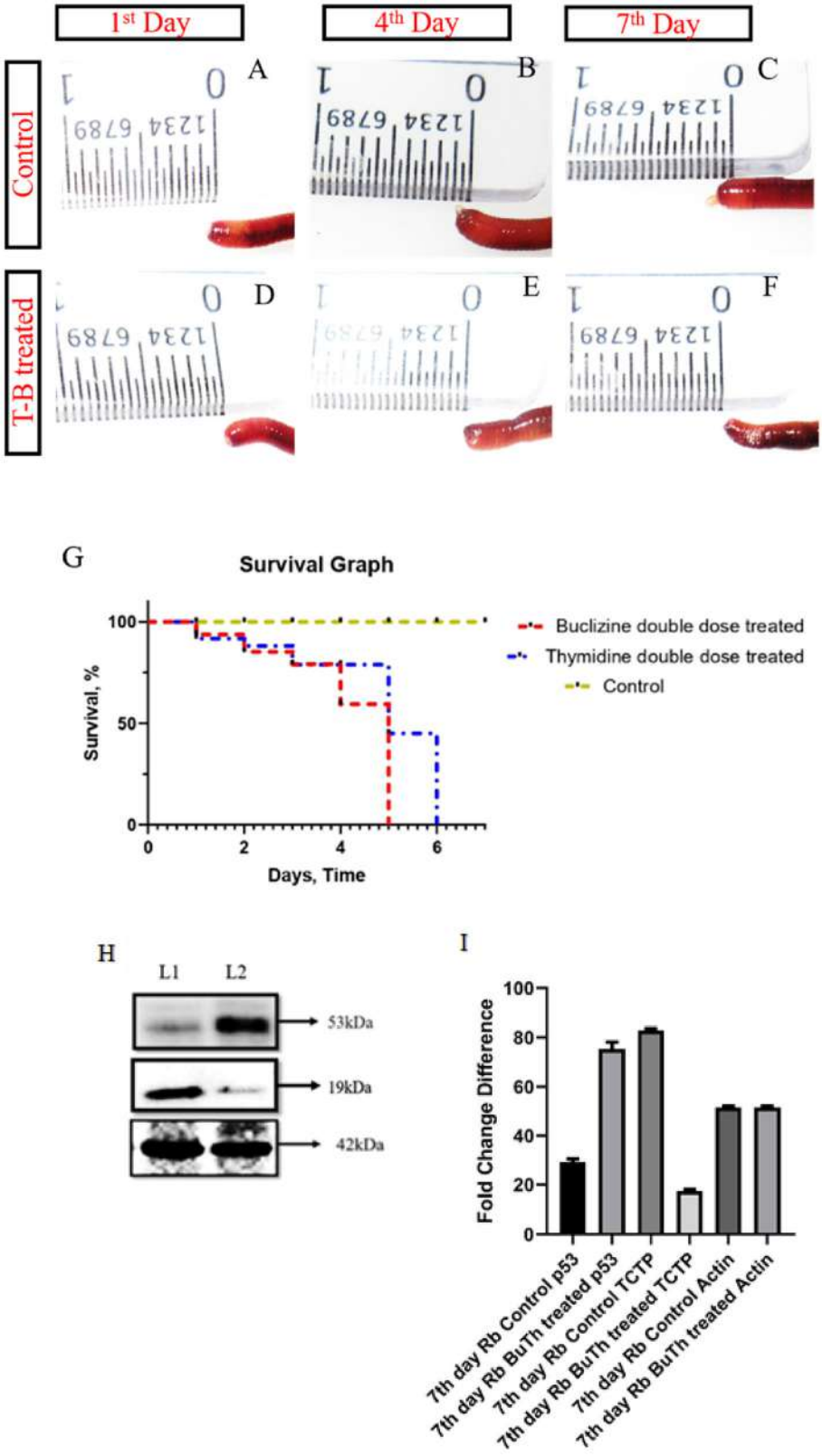

Fig. 4 Combinatorial injection of Buclizine and Thymidine: **A** control worm following day-1 post-amputation at 10th segment. **B** the amputated worms form blastema on the 4th day. **C** on the 7th day, the amputated worm forms elongated blastema. **D** Buclizine and Thymidine injected worm following 1st day of post-amputation. **E** complete inhibition of regeneration on 4th day of post-amputation in Buclizine and Thymidine injected worm. **F** Combinatorial injected worms show no sign of regeneration even after seven days of post-amputation. **G** Survival graph for the Control *P. excavatus*, buclizine, and Thymidine double dose-treated worms. After treatment, the live and dead worms on different days are counted and plotted in the survival (Kaplan–Meier) curve. Statistical analysis was accomplished using the log-rank test (Mantel-Cox), and the obtained p values < 0.05 were considered significant. **H** Expression of p53, TCTP, and β-actin in 8th day Control (L1) and 8th day Buclizine and Thymidine treated samples (L2). High expression of p53 and lower expression of TCTP was observed in Buclizine and Thymidine treated samples (p53–53 kDa; TCTP − 19 kDa; Actin − 42 kDa). **I** Band intensity of Western blotting image is quantified and represented with a bar diagram. Statistical significance is achieved when the p value is < 0.05

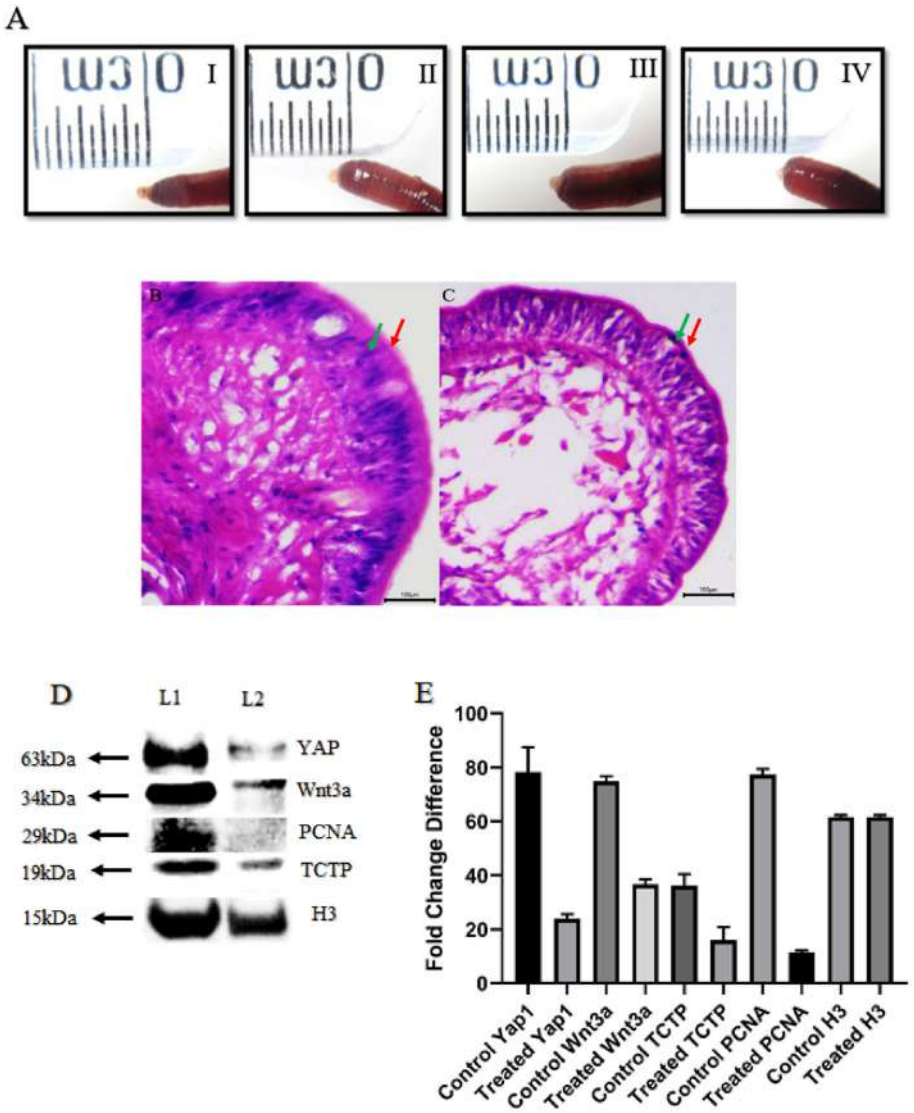

Fig. 5 TCTP and its connecting link with regenerative protein: **A** (I). Control amputated worm with 5th day bud. II, III and IV represent progressive regeneration suppression in Nutlin-3a injected worms with 5, 7, and 9 µg, respectively. **B** Histology of control 5th -day regenerative blastema with well-organized tissue structures has the most thickened outer and inner epithelial layer. **C** In Nutlin-3a injected worms, the 5th day bud is not well organized, loosely packed with internal bud tissues and thinner layers of the outer and inner epithelium. **D** Western blotting image represents that when compared to the control samples (7th day regeneration—Lane 1), all frame of regenerative key proteins was notably reduced in Nutlin-3a treated samples (7th day regeneration—Lane 2). Nutlin-3a is known for TCTP silencing, and according to the result, TCTP silence influences organ formation (YAP1), stem cell activation (Wnt3a) and cell proliferation (PCNA). E. Quantification of YAP1, Wnt3a, TCTP, PCNA and H3 expression are done based on the band intensity and represented using bar diagram. The experiments were repeated in triplicate to analyze the statistical significance, representing their value as mean ± SD. p value < 0.05 was considered statistically significant data. The red arrow represents the "Outermost epithelial layer"; the Green arrow represents the "Inner layer of epithelial tissue."

amputated at the post-clitellum segment (30th segment) can regrow as an individual worm. The data confirm that *P. excavatus* is a clitellum-independent worm that does not requires clitellum segments for their regeneration as it is necessary for clitellum-dependent worms [5]. The pre-blastema was observed within 48 h, and within another 24 h, the blastema developed into a well-developed structure and further developed rapidly in the following hours. The data represents that anterior head regeneration is more vigorous because it needs to restore all the vital organs like mouth, tubular heart, simple brain and other organ systems to survive and perform the normal functions. Following injection of 2mM Thymidine, the regeneration potential of the earthworm was suppressed to 1/3rd level, representing the earthworm. *P. excavatus* can perform regeneration to a certain extent by utilizing morphallaxis when blocking

epimorphosis. The epimorphosis mode of head regeneration was early reported in the earthworm *P. excavatus* [37], in which a high proliferative mass of cells forms the regenerative blastema. The blastema-like structure is observed in the arm regeneration of starfish, which adopts the intermediate mechanism of both morphallaxis and epimorphosis for their regeneration [44]. From histology, it confirms that the regenerative ability of the earthworm is suppressed in 2 mM Thymidine injected worms with a lack of development in their internal structures like functional mouth, septum, and segment elongation, which indirectly implies the factors or signals necessary for regeneration are not regulated correctly [45].

Following the pharmacological suppression of TCTP using an antihistamine drug, buclizine, the worm shows reduced regeneration ability which implies the critical role of TCTP in determining the regeneration ability of the worm. TCTP determines the cell fate on both ends, on a positive side through the influence of DNA damage and on a negative side as regulated by p53 [46]. The positive side of TCTP in determining the cell fate is revealed upon regeneration in that TCTP is upregulated on succeeding days of regeneration, and their pharmacological suppression hinders regeneration. TCTP also plays a crucial role in promoting the pathways related to cancer progression [47]. Therefore more studies are needed to understand their regulatory mechanism in determining the cell fate with controlled (Regeneration) and uncontrolled (Cancer) regulation upon many extracellular stimuli [48]. The modelled TCTP protein using earthworm sequences and their close interaction with buclizine and *in-vivo* results conclude that antihistaminics are the potent lead compounds in inhibiting the TCTP, which have a broad medicinal scope in treating cancers [48]. TCTP is a multi-functional protein that plays a crucial role in cell proliferation, cell growth, and apoptosis by interacting with many regulatory proteins [34]. TCTP's part is also well documented in regenerative models involving epimorphosis or cell proliferation [30, 34], but its role is not revealed in the aspect of morphallaxis. The combinatorial injection of 2 mM Thymidine and Buclizine inhibit both epimorphosis and TCTP protein, respectively, resulting in complete regeneration loss, but the worms survived without any physiological stress. The data confirms that 2 mM Thymidine injections block epimorphosis and conjoined inhibition of TCTP blocks morphallaxis, which can completely block the regeneration events in the earthworm, *P. excavatus.* The clitellum-independent worms have a vast regeneration ability because regeneration is not restricted or dependent only on the clitellum segments, and in such worms, TCTP governs both epimorphosis and morphallaxis. There are also high possibilities with more multi-functional ability of TCTP protein with animals with more regenerative ability and animals with less regenerative ability. In these aspects, research is needed to conclude it in the near future. Surprisingly in combinatorial injected amputated worms, the p53 level increased compared to the non-injected regenerating worms. p53 also reverses the cell cycle, allowing cells to repair their DNA and inducing apoptosis in severe DNA damage [49]. In the present study, the amputated worm is subjected to double stressful conditions, notably cell cycle arrest and TCTP suppression, and in that conditions, the worm expresses abundant p53, representing that p53 promotes cell survival to repair and rescue. Several *in-silico* and *in-vitro* research have examined buclizine as an inhibitor of TCTP, but neither study reported on *in-vivo* models [43, 50]. Here we reported the potential *in-vivo* interactions of Buclizine and TCTP with visible suppression of TCTP expression and regeneration in the earthworm model. TCTP is a multi-functional protein inhibiting them with Buclizine targets TCTP and interplays with the TCTP interacting proteins [51].

Unlike buclizine, the inhibitory effect of Nutlin-3a in targeting TCTP is well documented in many *in-vivo* models [30, 52, 53]. The delay of posterior segment regeneration and wound closure following amputation was reported in Nutlin-3a injected clitellum dependent, *Eudrilus eugeniae* earthworm. Similarly, in these present studies, upon anterior regeneration, Nutlin-3a suppresses regeneration; histologically, it is evident with the improper cellular package. The data indicates that TCTP is linked with many regenerations-associated proteins, such as those involved in cell proliferation, cellular morphallaxis, cell differentiation, apoptosis, immune response, stem cell activation, and organ development. Inhibiting TCTP with Nutlin-3a suppresses the regeneration mechanism together with influences from other proteins like PCNA (cell proliferation), Wnt3a (stem cell marker), and YAP1 (organ formation ruler and Hippo signaling). Following amputation, the microenvironment at the wound site provides signals for triggering regeneration and in which DNA damage-induced responses like apoptosis [54], stem cell migration [55] play a significant role in determining the regeneration potential. TCTP determines cell fate by regulating major cellular functions like apoptosis and proliferation [32, 56, 57]. Notably, the TCTP protein is known for its anti-apoptotic role [32, 58, 59] and also act as an apoptotic protein in some context of abrogate DNA repair [60]. Like TCTP, Wnt3a is also known for its pleiotropic cellular functions regulating cell proliferation, cell renewal, cellular differentiation, apoptosis, and motility [61]. Compared to other WNTs, Wnt3a is remarkably important in determining regeneration potential in *in-vitro*, *ex-vivo*, and *in-vivo* conditions [62]. Following pharmacological suppression of TCTP, the Wnt3a expression decreases and directly indicates the tight regulation between TCTP and Wnt3a upon

regeneration. The connective link between TCTP and β-catenin is reported in *in-vitro* and *in-vivo* cancer models [63], and in the present study the link between TCTP and Wnt3a upon regeneration is evident. The pharmacological inhibition of TCTP suppress the YAP1 signals upon regeneration and it represents the crosstalk between TCTP and YAP1. Regeneration occurs through a highly co-ordinated process and in that YAP/TAZ or Hippo pathway regulates the cell-cell interaction that determines the organ size and development [64]. YAP/TAZ complex also have a role in determining the cell fate by controlling the genes related with cell proliferation and apoptosis [65].

Apoptosis, stem cell activation, cellular proliferation, and organ development are essential for regeneration. Our studies conclude that TCTP governs both epimorphosis and morphallaxis during regeneration. Inhibiting TCTP impairs the regeneration mechanism by inhibiting all keyframes of regenerative proteins, including PCNA (proliferation), Wnt3a (Stem cell activation), and YAP1 (Hippo signaling). The cellular stress following pharmacological suppression of TCTP also initiates the p53 expression in the context of anti-apoptotic responses. Collectively, the present studies reveal the regulatory role of TCTP in connection with all critical regenerative proteins.

Acknowledgements Authors thank 'International Research Centre (IRC) of Sathyabama Institute of Science and Technology, Chennai' for providing support to carry out the research work. This work was supported by the DST-SERB-INDIA (Ref. No. ECR/2016/000956). The funding was provided by DST-SERB (Grant number ECR/2016/000956).

Author contributions KR (M-Tech, SRF, Ph.D Scholar) were involved in the writing original draft, conceptualization, data curation and figures. JDSC (Ph.D, Associate Professor (Research)) were involved in the writing original draft, conceptualization, data curation, investigation, supervision and project administration. KSC (M.Sc, M.Phil, OVDF Fellow, Ph.D Scholar) were involved in conceptualization and data curation. KM (Ph.D, Assistant Professor) were involved in bioinformatics analysis (protein preparation). PD (M.Sc), LN (M.Sc), SG (M.Sc) were involved in minor experiments.

Data availability statement The datasets used and/or analyzed during the present study are available from the corresponding author on reasonable request.

Declarations

Conflict of interest The authors declare no conflict of interest.

Ethical statement The experiments are carried out using lower invertebrate, earthworm therefore ethical statement is not needed. Necessary care is taken in experimental procedure that are intended to avoid unnecessary pain and sufering to the experimental animals.

References

1. Carlson BM. Principles of regenerative biology. Amsterdam: Elsevier; 2011.
2. Agata K, Saito Y, Nakajima E. Unifying principles of regeneration I: epimorphosis versus morphallaxis. Dev Growth Differ. 2007;49:73–8.
3. Morgan TH. Sex limited inheritance in Drosophila. Science. 1910;32:120–2.
4. Morgan TH. Regeneration. Stuttgart: Macmillan; 1901.
5. Selvan Christyraj JD, Azhagesan A, Ganesan M, Subbiah Nadar Chelladurai K, Paulraj VD, Selvan Christyraj JRS. Understanding the role of the Clitellum in the regeneration events of the earthworm Eudrilus Eugeniae. Cells Tissues Organs. 2019;208:134–41.
6. Sivasubramaniam S. The earthworm Eudrilus Eugeniae: a model organism for regenerative biology. J Genet Genomic Sci. 2021;6:23.
7. Owlarn S, Klenner F, Schmidt D, Rabert F, Tomasso A, Reuter H, et al. Generic wound signals initiate regeneration in missing-tissue contexts. Nat Commun. 2017;8:2282.
8. Pellettieri J. Regenerative tissue remodeling in planarians: the mysteries of morphallaxis. Seminars in cell and developmental biology. Amsterdam: Elsevier; 2019. p. 13–21.
9. Sugiyama T, Fujisawa T. Genetic analysis of developmental mechanisms in Hydra. II. Isolation and characterization of an interstitial cell-deficient strain. J Cell Sci. 1978;29:35–52.
10. Abnave P, Ghigo E. Role of the immune system in regeneration and its dynamic interplay with adult stem cells. Semin Cell Develop Biol. 2019;87:160–8.
11. Bergmann A, Steller H. Apoptosis, stem cells, and tissue regeneration. Sci Signal. 2010;3:re8.
12. Bosch TCG. Why polyps regenerate and we don't: towards a cellular and molecular framework for hydra regeneration. Dev Biol. 2007;303:421–33.
13. Suzuki M, Yakushiji N, Nakada Y, Satoh A, Ide H, Tamura K. Limb regeneration in Xenopus laevis froglet. ScientificWorldJournal. 2006;6:26–37.
14. Bodó K, Kellermayer Z, László Z, Boros Á, Kokhanyuk B, Németh P, et al. Injury-induced innate immune response during segment regeneration of the earthworm, Eisenia andrei. Int J Mol Sci. 2021;22:2363.
15. Liu T, Wang L, Chen H, Huang Y, Yang P, Ahmed N, et al. Molecular and cellular mechanisms of apoptosis during dissociated spermatogenesis. Front Physiol. 2017;8:188.
16. Fan Y, Bergmann A. Apoptosis-induced compensatory proliferation. The cell is dead. Long live the cell! Trends Cell Biol. 2008;18:467–73.
17. Huh JR, Guo M, Hay BA. Compensatory proliferation induced by cell death in the Drosophila wing disc requires activity of the apical cell death caspase dronc in a nonapoptotic role. Curr Biol. 2004;14:1262–6.
18. Jung Y, Witek RP, Syn WK, Choi SS, Omenetti A, Premont R, et al. Signals from dying hepatocytes trigger growth of liver progenitors. Gut. 2010;59:655–65.
19. Ryoo HD, Gorenc T, Steller H. Apoptotic cells can induce compensatory cell proliferation through the JNK and the wingless signaling pathways. Dev Cell. 2004;7:491–501.
20. Pérez-Garijo A, Steller H. Spreading the word: non-autonomous effects of apoptosis during development, regeneration and disease. Development. 2015;142:3253–62.
21. Fogarty CE, Bergmann A. Killers creating new life: caspases drive apoptosis-induced proliferation in tissue repair and disease. Cell Death Differ. 2017;24:1390–400.

22. Huang Q, Li F, Liu X, Li W, Shi W, Liu FF, et al. Caspase 3–mediated stimulation of tumor cell repopulation during cancer radiotherapy. Nat Med. 2011;17:860–6.
23. Llames S, García-Pérez E, Meana Á, Larcher F, del Río M. Feeder layer cell actions and applications. Tissue Eng Part B Rev. 2015;21:345–53.
24. Chera S, Ghila L, Wenger Y, Galliot B. Injury-induced activation of the MAPK/CREB pathway triggers apoptosis-induced compensatory proliferation in hydra head regeneration. Dev Growth Differ. 2011;53:186–201.
25. Fujimoto K, Yamamoto T, Kitano T, Abé SI. Promotion of cathepsin L activity in newt spermatogonial apoptosis induced by prolactin. FEBS Lett. 2002;521:43–6.
26. Li F, Huang Q, Chen J, Peng Y, Roop DR, Bedford JS, et al. Apoptotic cells activate the phoenix rising pathway to promote wound healing and tissue regeneration. Sci Signal. 2010;3:ra13.
27. Oka T, Adati N, Shinkai T, Sakuma K, Nishimura T, Kurose K. Bisphenol A induces apoptosis in central neural cells during early development of Xenopus laevis. Biochem Biophys Res Commun. 2003;312:877–82.
28. Pellettieri J, Fitzgerald P, Watanabe S, Mancuso J, Green DR, Sánchez Alvarado A. Cell death and tissue remodeling in planarian regeneration. Dev Biol. 2010;338:76–85.
29. Paul S, Balakrishnan S, Arumugaperumal A, Lathakumari S, Syamala SS, Arumugaswami V, et al. The transcriptome of anterior regeneration in earthworm Eudrilus eugeniae. Mol Biol Rep. 2021;48:259–83.
30. Subramanian ER, Gopi Daisy N, Sudalaimani DK, Ramamoorthy K, Balakrishnan S, Selvan Christyraj JD, et al. Function of translationally controlled tumor protein (TCTP) in Eudrilus eugeniae regeneration. PLoS One. 2017;12:e0175319.
31. Koziol MJ, Gurdon JB. TCTP in development and cancer. Biochem Res Int. 2012;2012:105203.
32. Rho SB, Lee JH, Park MS, Byun HJ, Kang S, Seo SS, et al. Anti-apoptotic protein TCTP controls the stability of the tumor suppressor p53. FEBS Lett. 2011;585:29–35.
33. Telerman A, Amson R. The molecular programme of tumour reversion: the steps beyond malignant transformation. Nat Rev Cancer. 2009;9:206–16.
34. Chen SH, Lu CH, Tsai MJ. TCTP is essential for cell proliferation and survival during CNS development. Cells. 2020;9: 133.
35. Amson R, Pece S, Lespagnol A, Vyas R, Mazzarol G, Tosoni D, et al. Reciprocal repression between P53 and TCTP. Nat Med. 2012;18:91–9.
36. Banik D, Chaudhuri PS. Regeneration ability in seventeen top soil and sub soil earthworm species. J Environ Biol. 2017;38:393.
37. Bae YS, Kim J, Yi J, Park SC, Lee HY, Cho SJ. Characterization of *Perionyx excavatus* development and its head regeneration. Biology (Basel). 2020;9:273.
38. Cho SJ, Lee MS, Tak ES, Lee E, Koh KS, Ahn CH, et al. Gene expression profile in the anterior regeneration of the earthworm using expressed sequence tags. Biosci Biotechnol Biochem. 2009;73:29–34.
39. Martinez VG, Menger GJ 3rd, Zoran MJ. Regeneration and asexual reproduction share common molecular changes: upregulation of a neural glycoepitope during morphallaxis in Lumbriculus. Mech Dev. 2005;122:721–32.
40. Chellathurai Vasantha N, Rajagopalan K, Selvan Christyraj JD, Subbiahanadar Chelladurai K, Ganesan M, Azhagesan A, et al. Heat-inactivated coelomic fluid of the earthworm Perionyx excavatus is a possible alternative source for fetal bovine serum in animal cell culture. Biotechnol Prog. 2019;35:e2817.
41. Gopi Daisy N, Subramanian ER, Selvan Christyraj JD, Sudalai Mani DK, Selvan Christyraj JR, Ramamoorthy K, et al. Studies on regeneration of central nervous system and social ability of the earthworm Eudrilus eugeniae. Invert Neurosci. 2016;16:6.
42. Johnson Retnaraj Samuel SC, Elaiya Raja S, Beryl Vedha Y, Edith Arul Jane A, Amutha K, Dinesh SM, et al. Autofluorescence in BrdU-positive cells and augmentation of regeneration kinetics by riboflavin. Stem Cells Dev. 2012;21:2071–83.
43. Seo EJ, Efferth T. Interaction of antihistaminic drugs with human translationally controlled tumor protein (TCTP) as novel approach for differentiation therapy. Oncotarget. 2016;7:16818.
44. Yokoyama H, Ogino H, Stoick-Cooper CL, et al. Wnt/β-catenin signaling has an essential role in the initiation of limb regeneration. Dev Biol. 2007;306:170–8.
45. Michalopoulos GK. Liver regeneration. Liver Biol Pathobiol. 2020. https://doi.org/10.1002/9781119436812.ch45.
46. Acunzo J, Baylot V, So A, Rocchi P. TCTP as therapeutic target in cancers. Cancer Treat Rev. 2014;40:760–9.
47. Bommer UA, Kawakami T. Role of TCTP in cell biological and disease processes. Cells. 2021;10:2290.
48. Seo EJ, Fischer N, Efferth T. Role of TCTP for cellular differentiation and cancer therapy. Results Probl Cell Differ. 2017;64:263–81.
49. Feroz W, Sheikh AMA. Exploring the multiple roles of guardian of the genome: P53. Egypt J Med Hum Genet. 2020;21:1–23.
50. Kumar R, Maurya R, Saran S. Identification of novel inhibitors of the translationally controlled tumor protein (TCTP): insights from molecular dynamics. Mol Biosyst. 2017;13:510–24.
51. Bommer U-A, Telerman A. Dysregulation of TCTP in biological processes and diseases. Cells. 2020;9:1632.
52. Zuber J, Rappaport AR, Luo W, et al. An integrated approach to dissecting oncogene addiction implicates a myb-coordinated self-renewal program as essential for leukemia maintenance. Genes Dev. 2011;25:1628–40.
53. Kang JH, Lee SH, Lee JS, Oh SJ, Ha JS, Choi HJ, et al. Inhibition of transglutaminase 2 but not of MDM2 has a significant therapeutic effect on renal cell carcinoma. Cells. 2020;9:1475.
54. Ryoo HD, Bergmann A. The role of apoptosis-induced proliferation for regeneration and cancer. Cold Spring Harb Perspect Biol. 2012;4:a008797.
55. Sahu S, Sridhar D, Abnave P, Kosaka N, Dattani A, Thompson JM, et al. Ongoing repair of migration-coupled DNA damage allows planarian adult stem cells to reach wound sites. Elife. 2021;10: e63779.
56. Hsu YC, Chern JJ, Cai Y, Liu M, Choi KW. Drosophila TCTP is essential for growth and proliferation through regulation of dRheb GTPase. Nature. 2007;445:785–8.
57. Telerman A, Amson R. TCTP/tpt1-Remodeling signaling from stem cell to disease. Berlin: Springer; 2017.
58. Bommer UA, Thiele BJ. The translationally controlled tumour protein (TCTP). Int J Biochem Cell Biol. 2004;36:379–85.
59. Lee HJ, Song KH, Oh SJ, Kim S, Cho E, Kim J, et al. Targeting TCTP sensitizes tumor to T cell-mediated therapy by reversing immune-refractory phenotypes. Nat Commun. 2022;13:2127.
60. Omabe K. Translationally controlled tumor protein: a key target to abrogate DNA repair and therapeutic resistance in cancer. J Cancer Res Ther Oncol. 2022;10:1–17.
61. He S, Lu Y, Liu X, Huang X, Keller ET, Qian CN, et al. Wnt3a: functions and implications in cancer. Chin J Cancer. 2015;34:1–9.
62. Chang CY, Liang MZ, Wu CC, Huang PY, Chen HI, Yet SF, et al. WNT3A promotes neuronal regeneration upon traumatic brain injury. Int J Mol Sci. 2020;21:1463.
63. Gu X, Yao L, Ma G, Cui L, Li Y, Liang W, et al. TCTP promotes glioma cell proliferation in vitro and in vivo via enhanced β-catenin/TCF-4 transcription. Neuro Oncol. 2014;16:217–27.
64. Halder G, Johnson RL. Hippo signaling: growth control and beyond. Development. 2011;138:9–22.

65. Varelas X. The Hippo pathway effectors TAZ and YAP in development, homeostasis and disease. Development. 2014;141:1614–26.

Publisher's Note Springer Nature remains neutral with regard to jurisdictional claims in published maps and institutional affiliations.

Springer Nature or its licensor (e.g. a society or other partner) holds exclusive rights to this article under a publishing agreement with the author(s) or other rightsholder(s); author self-archiving of the accepted manuscript version of this article is solely governed by the terms of such publishing agreement and applicable law.

scientific reports

Check for updates

OPEN

Exploring the effect of UV-C radiation on earthworm and understanding its genomic integrity in the context of H2AX expression

Karthikeyan Subbiahanadar Chelladurai[1], Jackson Durairaj Selvan Christyraj[1]✉, Ananthaselvam Azhagesan[1,2], Vennila Devi Paulraj[1], Muralidharan Jothimani[1,3], Beryl Vedha Yesudhason[1], Niranjan Chellathurai Vasantha[1], Mijithra Ganesan[1], Kamarajan Rajagopalan[1], Saravanakumar Venkatachalam[1], Johnson Benedict[1], Jemima Kamalapriya John Samuel[4] & Johnson Retnaraj Samuel Selvan Christyraj[1]✉

Maintaining genomic stability is inevitable for organism survival and it is challenged by mutagenic agents, which include ultraviolet (UV) radiation. Whenever DNA damage occurs, it is sensed by DNA-repairing proteins and thereby performing the DNA-repair mechanism. Specifically, in response to DNA damage, H2AX is a key protein involved in initiating the DNA-repair processes. In this present study, we investigate the effect of UV-C on earthworm, *Perionyx excavatus* and analyzed the DNA-damage response. Briefly, we expose the worms to different doses of UV-C and find that worms are highly sensitive to UV-C. As a primary response, earthworms produce coelomic fluid followed by autotomy. However, tissue inflammation followed by death is observed when we expose worm to increased doses of UV-C. In particular, UV-C promotes damages in skin layers and on the contrary, it mediates the chloragogen and epithelial outgrowth in intestinal tissues. Furthermore, UV-C promotes DNA damages followed by upregulation of H2AX on dose-dependent manner. Our finding confirms DNA damage caused by UV-C is directly proportional to the expression of H2AX. In short, we conclude that H2AX is present in the invertebrate earthworm, which plays an evolutionarily conserved role in DNA damage event as like that in higher animals.

For the survival of organisms, maintenance of genome integrity is crucial and inevitable[1]. In the context of evolution, higher organisms have developed complex mechanisms to identify and repair DNA breaks[2,3]. The DNA damage engages with a series of cellular response events that result in either cell cycle arrest or in some extreme cases it leads to apoptosis[4]. When the DNA damage occurs, its hurried and synchronized action of various signaling pathways, including cell-cycle checkpoint activation[5,6], histone modification near the site of the break[7], chromatin remodeling[8], cohesins modulation[9], and activation of DNA-repair proteins[6]. Many of the defects in these pathways lead to several disorders in human[5]. The genome integrity is challenged by several factors and one of the main factors is UV radiation[10]. Therefore, studies on UV radiation on biological system is getting more attention.

Ultraviolet (UV) is one of the components of solar radiation, which is classified into UV-A (320–400 nm), UV-B (280–320 nm), and UV-C (200–280 nm)[11]. The UV-C and most of the UV-B do not have the ability to reach Earth because it is stopped by the stratospheric ozone layer. Therefore, only UV-A and slight UV-B reach the Earth[12]. As reported already, the total stratospheric ozone layer depleted by 10% so that the UV-B reaching

[1]Regeneration and Stem Cell Biology Lab, Centre for Molecular and Nanomedical Sciences, International Research Centre, Sathyabama Institute of Science and Technology, Chennai 600119, Tamilnadu, India. [2]Present address: Centre for Nanobiotechnology, Vellore Institute of Technology, Vellore 632014, Tamilnadu, India. [3]Present address: Department of Bioinformatics, Science Campus, Alagappa University, Karaikudi 630004, Tamilnadu, India. [4]Department of Biotechnology, Anna University of Technology, Tiruchirappalli 620024, Tamilnadu, India. ✉email: jacksondurairaj@sathyabama.ac.in; johnnbt@sathyabama.ac.in

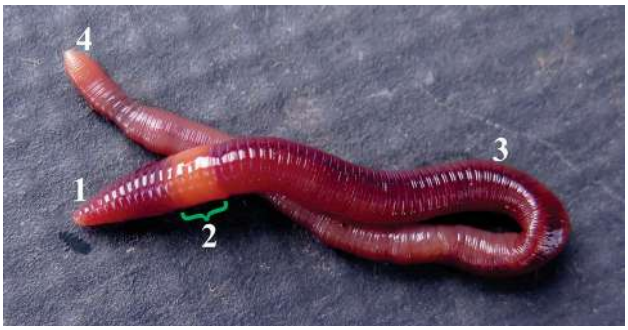

Figure 1. *Morphology of earthworm, P. excavatus.* The anterior region of the worm (1 to 12th segments) is called as head, which comprises of prostomium, brain, heart, seminal vesicles, testis (1), Muscular thick portion that occurs behind the head region is called as clitellum and it is located in between 13–17th segment (2), Following clitellum region, there are no notable organ system present in the post clitellum region except a pair of prostate gland that lies on 18th segment (3). The posterior end of the worm is called tail region (4).

the Earth's surface increased by 20%[13]. However, a recent study shows that there is some recovery from ozone depletion; but that is not significant except in Antarctica[14]. Although UV-C has not reached the Earth's surface from the solar light, many man-made activities like arc-welding torches[15], mercury lamps, UV sanitizing bulbs[16] emit UV-C. Similarly, UV-C is highly used for post-harvest improvement[17] and also used in food industries as disinfection[18]. Even in the COVID-19 pandemic, people are suggesting to use low dose of UV-C (222 nm) to reduce the ambient level of airborne viruses with positive results coming out in in-vitro experiments[19]; but how safe it is in the real-world environment is questionable. UV-A light is poorly absorbed by most biomolecules; however, it can damage DNA indirectly through the photosensitizer molecules. UV-B is directly absorbed by nucleic acids and generates reactive oxygen species, oxidative stress, and inducing DNA damage. UV-C is also strappingly absorbed by nucleic acids of purine as well as pyrimidine bases and generate excited-state species, which leads to DNA damage and results in cell death or mutation[20,21].

H2A histone family member X is a type of histone protein and referred to as H2AX. The phosphorylated H2AX (γH2AX) foci formation is a potent tool used to study DNA double standard break formation and repair after genomic damage, change in chromosome dynamics, and signalling mechanisms associated with DNA damage response[22,23]. H2AX is highly conserved from *Giardia intestinalis* to *Homo sapiens*[24]. Reports clearly suggest that UV exposure induces H2AX[25]. In addition, solar radiation effects on the living system have been highly discussed[26,27]; but limited studies discussed the effect of UV-C in animals. Concerns with high depletion of the ozone layer and increasing uses of artificial UV-C lead us to showcase the importance of UV-C effect on the animal system.

Earthworms are hermaphrodite, segmented, tubular worm, which come under phylum-Annelida, class-Oligochaeta[28]. These are widely used as a model system for regeneration[29] and toxicology studies, worldwide[30]. In the present study, we investigated the effect of UV-C on earthworm, *Perionyx excavatus* and its impact on genome integrity. In addition, we explored the presence of H2AX protein in earthworm and confirm its role in DNA repairing event.

Results

Effect of UV-C on earthworm behavior. Earthworms are used as an animal model for the current experimental setup as described in materials and methods section. *P. excavatus* like other species of earthworm has a segmented body including head, clitellum, post clitellum and tail region (Fig. 1), and it looks smooth and shiny (Figs. 1,2A). Before proceeding with the experiments, it is essential to know the behavior of the earthworm under daylight and night conditions. In the night condition, the crawling speed of *P. excavatus* is very slow and noted as relaxed crawling. But under the daylight condition at laminar airflow, it looks slightly stressed and the crawling speed is slightly higher when compared to the night condition. Interestingly, if you switch off the normal light and switch on the UV-C light, it shows the vigorous altered behavior with a lift up of one-fifth of their body from the platform and shaking it (Supplementary Video S1). Generally, whenever they gets stressed, they start to release a thick yellow colored coelomic fluid through their dorsal pores (Fig. 2B). Notably, earthworm crawling speed doubles when they are exposed to increasing dose of UV light; but once it is over the optimal tolerance level, that is, UV exposure dose of 5 min hinders their active crawling along with secretion of a flimsy, colorless coelomic fluid around their dorsal surface (Fig. 2C). However, it is visible in white color patches following a 15 h post UV-C treatment, which shows the increasing appearance on the dorsal skin respectively from 2 min (Fig. 2D), 3 min (Fig. 2E), and 5 min (Fig. 2F). But the similar formation of white color patches on the dorsal surface of the worm is not observed in control and 1 min UV-C exposed worms.

Survival ability of earthworm following UV-C exposure. All the groups of UV treated worms (1, 2, 3, and 5 min) survive till 15 h of post-UV-C treatment. But after 15–20 h of post-UV treatment, we can observe worm mortality and notable skin damage. In 1 min UV-C-treated group, slight skin burns are visible in 1/10 worms, but all other worms are alive and active. In 2 min UV-C-treated group, 2/10 worms die and another 2/10

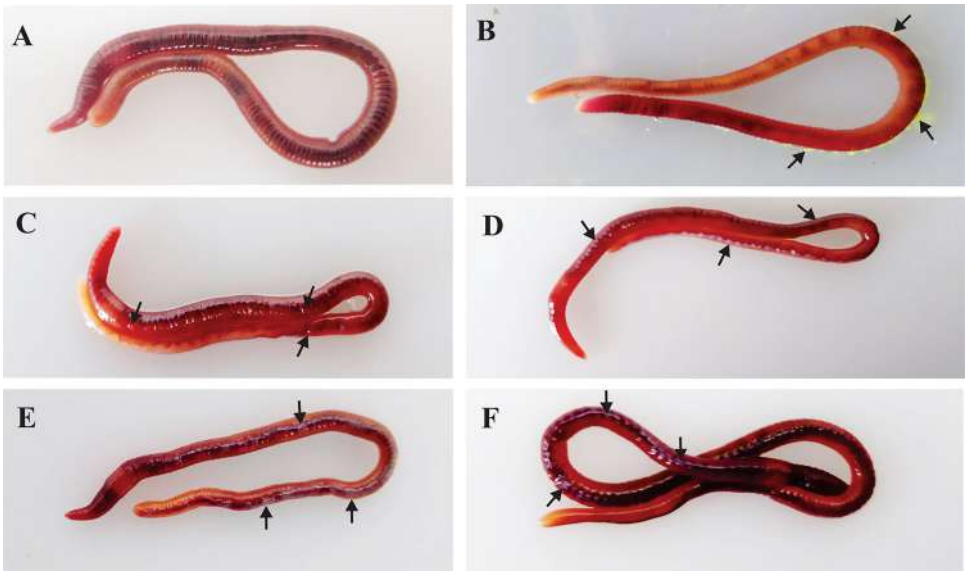

Figure 2. Releasing of earthworm coelomic fluid in different condition. (**A**) Control worms without stress not releasing coelomic fluid on the dorsal surface. (**B**) Releasing of coelomic fluid in 10% ethanol. (**C**) Releasing of coelomic fluid after 5 min of UV-C treatment. (**D**–**F**) White color patch of coelomic fluid visible after 15 h of post UV-C exposure of 2, 3, and 5 min, respectively.

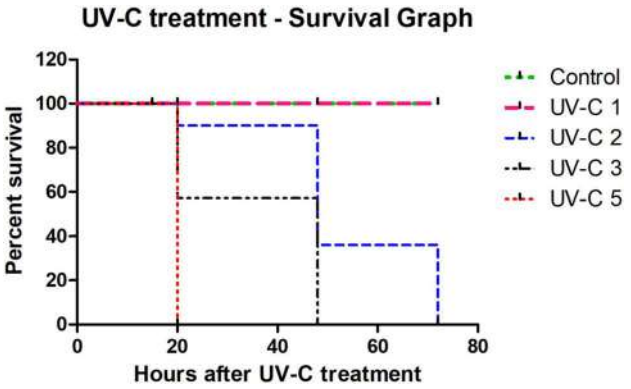

Figure 3. Mortality rate after 20 h of post-UV-C treatment at various doses. No individual worms died in the control group. When the earthworms are exposed to 1 min of UV-C exposure, no mortality is observed. But after exposure to higher doses of (2, 3, and 5 min) exposure, it shows the mortality rate of 20%, 40%, and 100%, respectively.

worms are highly damaged in the outer tissue layer and the remaining 6/10 worms are alive. In 3 min UV-C-treated group, 4/10 worms die, 2/10 worms are highly damaged in the outer skin layer, and the remaining 4/10 worms are alive. But we observe 100% mortality in 5 min UV-C-treated worms after 20 h of post UV exposure (Fig. 3). Similarly, the entire group of worms in 2 min and 3 min UV-treated groups died within 72 and 48 h, respectively. The 1 min UV-C-treated worms show 100% UV tolerance without any mortality similar to control group.

Phenotypic observation. After 20 h of post UV treatment, except in the control worm (Fig. 4A–C), phenotypic changes are observed in all other groups of worms. In 1 min UV-treated group, 1/10 worms show slight skin burn (Fig. 4D,E). But in all other groups (2, 3, and 5 min UV-exposed worms), distinct phenotypic changes are observed as shown in Fig. 4G–O. In 2 min UV-treated worms, the following notable characteristic changes are observed: (1) Skin burns observed in all the worms (Fig. 4G,H); (2) Segment swellings observed in 1/10 worms (Fig. 5A); (3) Cleavage furrow formation in 4/10 worms (Figs. 4G,5C); and (4) Damaged tail detaches by autotomy 1/10 worms (Figs. 4G,5B). In 3 min UV-C-treated worms, tissue inflammation is observed in post-clitellum segments with distinguished tissue color change from brownish to slight yellow in 6/10 worms (Fig. 4J,K). In 2/10 worms, the cleavage furrow formed in the post-clitellum segment proceed further to form detached segments (Fig. 5D). In 5 min UV-treated group, severe tissue inflammation is observed in the post-clitellum

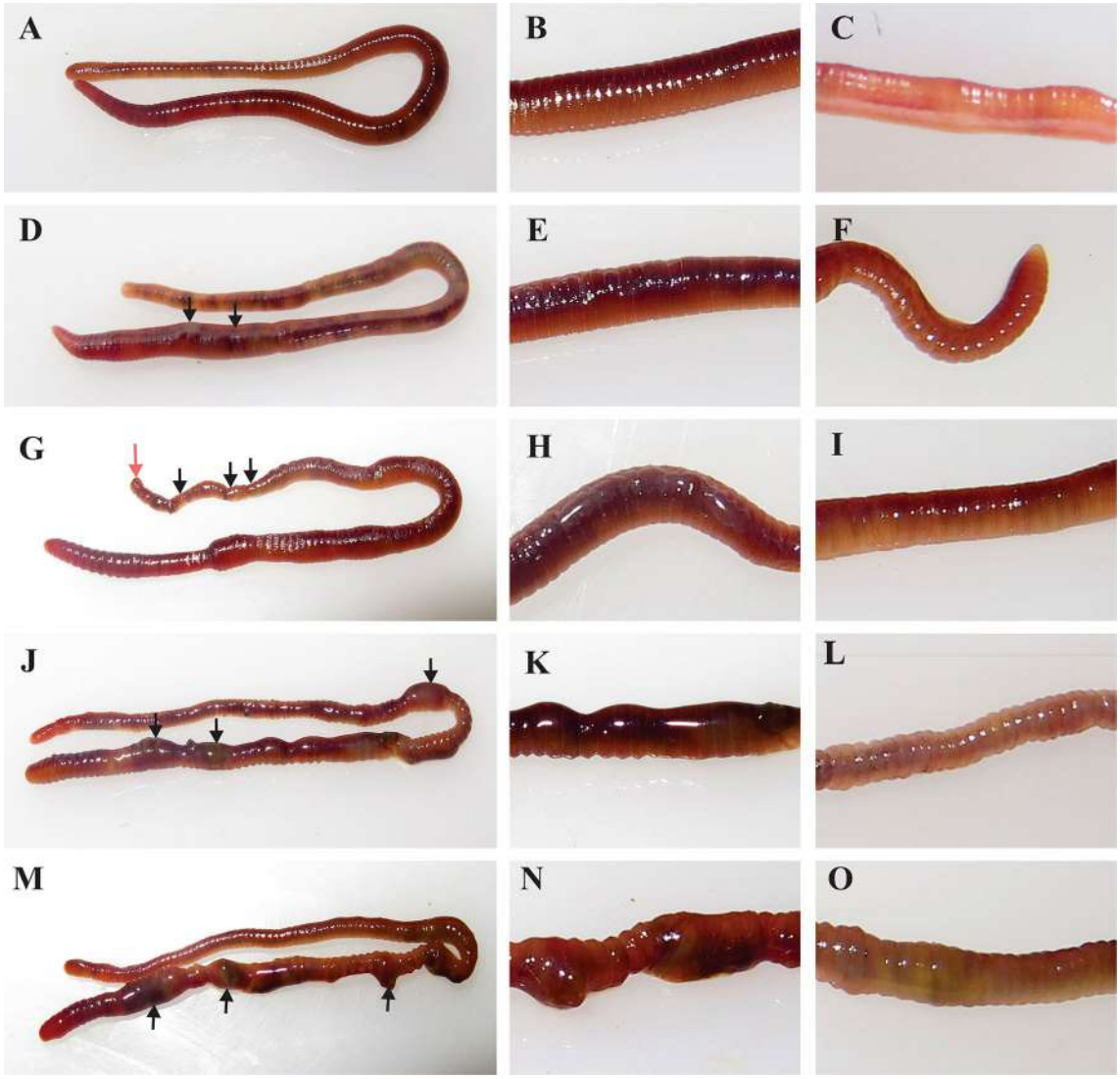

Figure 4. Phenotypic changes in the earthworm, *P. excavatus* after 20 h of post-UV-C exposure. (**A**–**C**), (**D**–**F**), (**G**–**I**), (**J**–**L**) and (**M**–**O**) respectively from control, 1, 2, 3, and 5 min UV-C-treated worms. Control worms without exposure to UV-C (**A**–**C**). Slight burn occur in UV-C, 1 min treated worms (**D**, **E**); autotomy (red arrow), and cleavage furrow (black arrow) visible in UV-C, 2 min treated worms (**G**); tissue inflammation visible in UV-C, 3 min treated worms (**J**, **K**); High inflammatory, tissue segments (dead worm) appear in UV-C, 5 min treated worms (**M**, **N**). No tissue damage observed in control post clitellum region (**B**). The damage is clearly visible in the post clitellum region and it increases from 1, 2, 3 and 5 min UV-C treated worms respectivily **E**, **H**, **K** and **N**. No color change in control group tail (**C**). The yellow color appears and gradually increases in the tail region of the 1, 2, 3, 5 min UV-C treated worms respectivily from **F**, **I**, **L** and **O**.

segments with a distinct knot-like structure formation in 8/10 worms (Fig. 4M,N). In the knot formation site, the brownish skin color turns to blackish pale yellow color. Another interesting observation noticed is in the tail region of the UV-C-treated worm where the tissue color gradually changes from pale yellow to greenish yellow, which is more prominently visible in 5 min-treated group (Fig. 4C,F,I,L,O). The crawling speed of the worms slowdown in the 2 and 3 min UV-C-treated group with high incidence of slow crawling observed in highly damaged. Similarly, in 3 and 5 min UV-C-treated groups, 3/10 and 2/10 worms observe high weight loss along with dehydrated tissue nature (Fig. 5E). The knot formation and degeneration occur in 5 min UV-C-treated group at posterior segments, but no such changes are visible in the anterior region from prostomium to clitellum region (Fig. 5F).

Pathological effects of UV-C. Histological sectioning of control worm tissue architecture show no tissue damage in intestinal cavity, intestinal epithelial layer (Fig. 6A) and in three skin layers, namely epidermal layer, circular muscle, and longitudinal layer. Additionally, the coelomic cavity, which occurs in between intestinal tissue and the skin tissue layers shows free-flow space and slight accumulation of coelomocytes (Fig. 6B,C). In 1 min UV-C-treated groups, no substantial damage or change is observed (Fig. 6D–F) when compared to

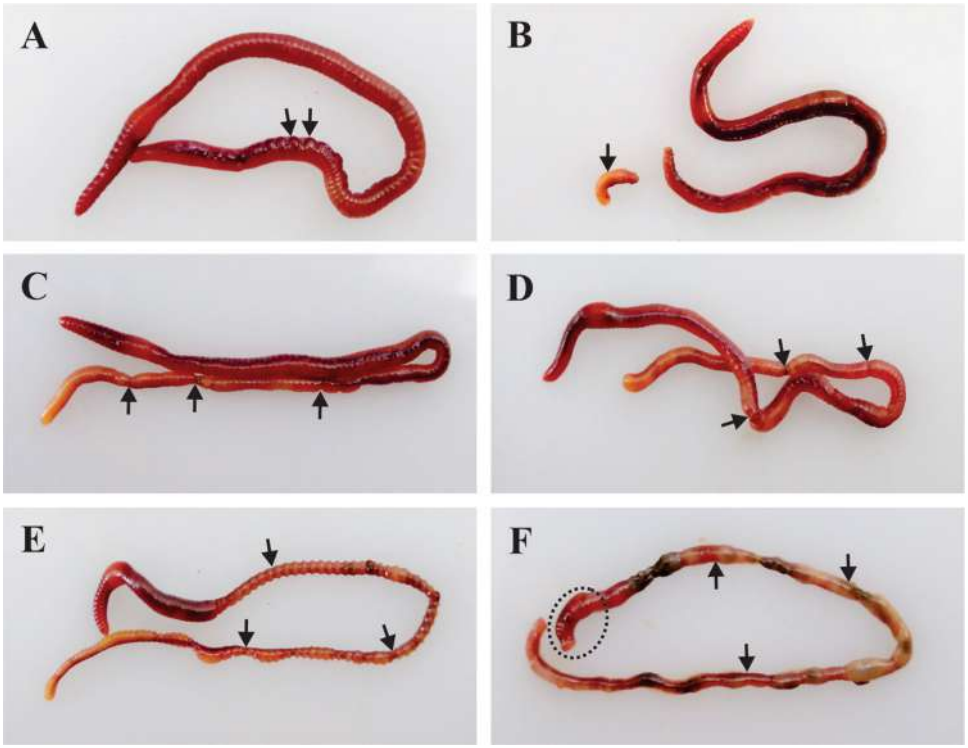

Figure 5. Phenotypic changes observed in earthworm, *P. excavatus*. After 20 h of post-UV-C exposure, tissue bulges are observed in some segments (**A**). Small pieces of tail segments are separated from the worm by autotomy (**B**). Cleavage furrow appears in the post clitellum region (**C**). Cleavage furrow almost proceeds with formation of detached segments (**D**). In the post clitellum region, the worm segment is fully dehydrated (**E**). Dead worms fully degenerated in the posterior region, but not in the anterior region from mouth to clitellum segments; but prostomium gets damaged heavily (**F**).

control, but in the dorsal side of the skin, the epithelial flip structure is disturbed notably (Fig. 6E). However, in 2 min UV-C-treated group, the coelomic fluid cavity is highly reduced (Fig. 6G–I); the epidermis is highly damaged with collapsed flip structure; circular muscle layer shows slight damage and increased tissue pattern of longitudinal tissue layer on the dorsal side (Fig. 6H). Moreover, notable coelomocyte accumulation is observed in both dorsal and ventral side (Fig. 6H,I). Interestingly, in 3 min UV-C-treated group, the intestine gets shrunk, no space is observed in between the adjacent intestinal epithelium and thereby completely blocking the passage of food (Fig. 6J). Additionally, the outgrowth of chloragogen tissue layer at the dorsal side pushes the coelomocyte towards the damaged skin layer and thereby seals the entire tissue layer and blocks the free flow of coelomic fluid (Fig. 6J,K). Overall, the dorsal side of the worm is highly exposed to UV-C and receives more damage with an enlarged epithelial layer together with the collapsed flip structure. UV-C-induced damages are commonly observed in the circular muscle layer with collapsed structure. In high UV-C dose, reduced tissue pattern of longitudinal skin layer is also observed. The skin layer together with chloragogen tissue and coelomic fluid make it a condensed stagnated structure (Fig. 6K). Similarly, at the ventral side, stagnant or condensed coelomic fluid towards the chloragogen tissue layer is visible and notably the coelomic fluid free flow space in between ventral skin tissue and the longitudinal layer is highly reduced (Fig. 6L). Similarly, in 5 min UV-treated group, the inner side of intestinal epithelial tissues fuses at many sites preventing the free flow of food (soil). The outer face of intestinal tissue outgrowth merges with the overlaying longitudinal cell layers along with the coelomocytes (Fig. 6M). The dorsal and ventral sides of the 5 min-treated group are similar with the 3 min-treated group (Fig. 6N,M). However, there is an unknown visible structure observed (Fluorescent green arrow) in-between the intestinal tissue and the accumulated coelomocytes of the ventral side of the worm (Fig. 6L,O).

UV-C effect on earthworm genome integrity. The genome integrity of the earthworm is analyzed by DNA fragmentation assay. DNA is isolated from UV-C-treated and the control group of earthworms and resolved in agarose gel electrophoresis. In the control group, genomic DNA is clearly visible as a single band, but in the UV-C-treated groups, DNA fragments are visible as a sheared band because of the fragmented DNA. The fragmentation gradually increases from UV-C 1 min- to UV-C 5 min-treated group. The DNA fragmentation is high in the UV-C 3 min- and 5 min-treated group (Fig. 7A). The data confirms that the earthworm DNA damage is increased by increasing the UV-C dose. Further to confirm the UV-C-induced DNA damage, alkaline comet assay is performed using the DNA that are isolated from the UV-C treated earthworm tissue, which shows DNA damage increases in a dose-dependent manner which are revealed through the increasing size of the comet length. In control, the DNA is visible as circular in structure, but in 1 min-treated group it shows a slight halo

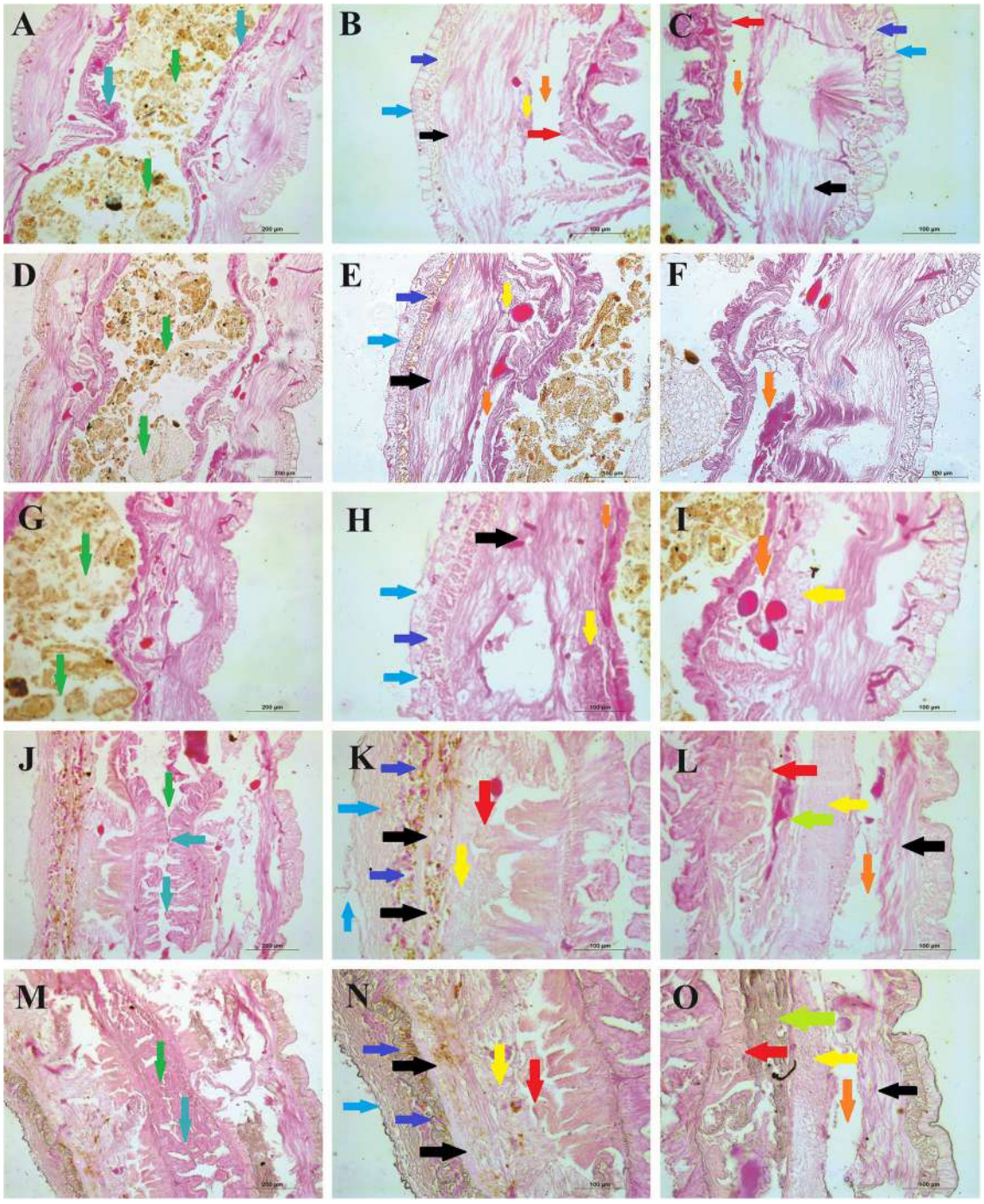

Figure 6. Longitudinal tissue structure of *P. excavatus* after 20 h of different doses of UV exposure (post clitellum section—figure panel (**A**), (**D**), (**G**), (**J**), and (**M**)—200 µm; dorsal side—figure panel (**B**), (**E**), (**H**), (**K**), and (**N**)—100 µm; ventral side—figure panel (**C**), (**F**), (**I**), (**L**), and (**O**)—100 µm). (Arrows green—intestinal cavity, blue—intestinal epithelium, sky blue—skin epithelium, violet—circular muscle, black—longitudinal tissue, yellow—coelomocyte, orange—coelomic fluid cavity, red—chloragogen tissue, fluorescent green—unknown structure). Longitudinal sections (LS) of *P. excavatus* without UV-C exposure (**A**–**C**) clearly show all the tissue structures without any damage. In 1 min UV-C-treated worms (**D**–**F**), (**D**)—the visible space in the intestinal cavity, (**E**)—flip structure collapsed in epithelial layer others are similar to (**B**), (**F**)—no notable changes in ventral side similar with (**C**). The 2 min-treated worms show (**G**–**I**) (**G**)—similar to control, (**H**)—high damage in epithelial tissue and slight damage in circular muscle tissue, slight increase in size in the longitudinal tissue layer, no substantial space of coelomic fluid free flow space, (**I**)—reduction of coelomic fluid cavity and slightly increased accumulation of coelomocytes. UV-C for 3 min (**J**–**L**), (**J**)—highly reduced intestinal cavity space, overgrowth of intestinal epithelial tissues, (**K**)—fully collapsed and increased structure of epithelial, slight structural changes and damages of circular muscle, change in tissue pattern and reduction in size of longitudinal tissue layer, high production or accumulation of coelomocyte, substantial growth of chloragogen tissue layer, (**L**)—in ventral side, chloragogen tissue overgrowth, unknown structure (fluorescent green), accumulation of coelomocyte, coelomic fluid cavity space reduced the size of longitudinal tissue layer. Similarly, in 5 min UV-C-treated group (**M**–**O**), (**M**)—intestinal cavity fully blacked, intestinal epithelial fused from both side, (**N**)—dorsal side is similar to (**K**), (**O**)—ventral side is similar with (**L**).

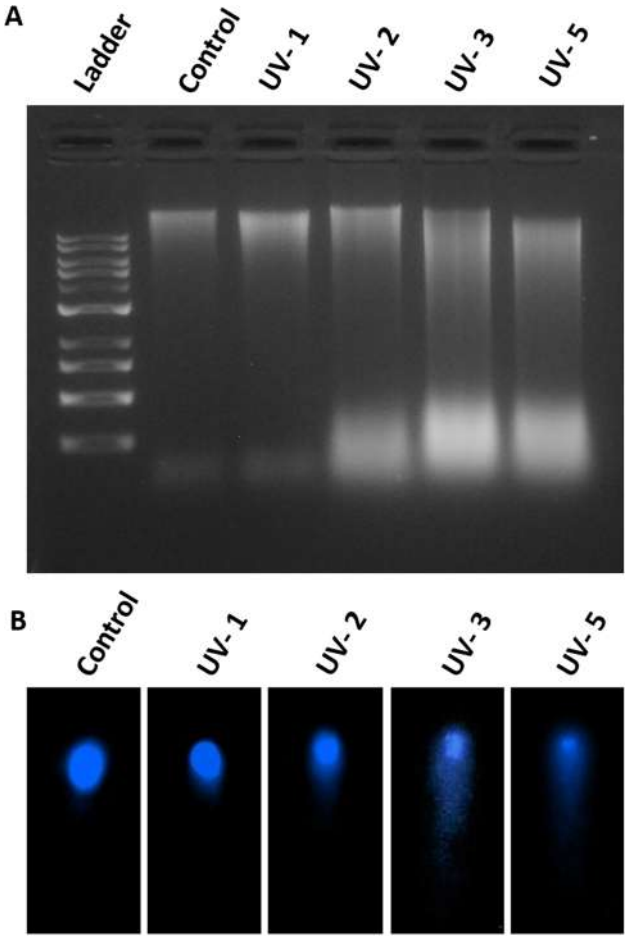

Figure 7. DNA fragmentation assay and Comet Assay. (**A**) DNA fragmentation assay—ladder (1 kb), Control group DNA with a single clear band and from 1, 2, 3, and 5 min UV-C-exposed earthworms, DNA are fragmented and come with dragged structure. The DNA fragmentation dragged is high in UV-C 3 and 5 min-treated groups. (**B**) Comet assay—in control group, the DNA appears in a proper round structure whereas in 1–5 min UV-C-treated group, it shows increased tail movement.

structure around the comet head. Moreover, very few comet tails are visible in the same group. However, comet tail gradually increases from 2 min, 3 min, and 5 min UV-C-treated group (Fig. 7B) in parallel to the decrease in comet head. From the results it is evident that DNA single strand break and increased length of tail, which referred to the high DNA damage. These long comet tails are observed more in number in UV-C 3 and 5 min-treated animals.

Effect of UV-C on H2AX and β-actin. To study the expression of H2AX and β-actin following UV-C treatment, Western blot analysis is performed. Briefly, protein lysate is prepared from the control and UV-C-treated earthworms and subject to Western blotting against H2AX and β-actin antibodies. The data shown in Fig. 8A proves that upon exposure to increasing dose of UV-C, *P. excavatus* show gradual upregulation of H2AX expression from UV-C 1 min-treated to UV-C 3 min-treated groups. H2AX in the 1, 2- and 3-min UV-C-treated groups is overexpressed to a fold of 1.54, 2.14 and 3.26 times higher respectively than the control group (Fig. 8B). Similarly, β-actin, normally used as a loading control is also elevated in UV-C-treated groups. The expression level of β-actin is increased to 1.12, 1.96, 1.85 folds in UV- 1, 2, 3 min treated group respectively than in the control worm (Fig. 8B). Protein sample is not obtained from the 5 min-treated group because no more worms are alive in 5 min UV-C treated group following 20 h.

Discussion

Significance of coelomic fluid in earthworm survival. In this present study, the earthworm *P. excavatus* is used as an animal model to study the impact of UV-C on earthworm morphology and genomic integrity. Generally, if earthworms are under stress condition, they release coelomic fluid, which usually possesses several immune defence-related biological functions[31]. The earthworm, *P. excavatus* coelomic fluid is yellow in color due to the presence of autofluorescence riboflavin in the type of coelomocyte called eleocytes[32] and the viscosity of the fluid is very high (Fig. 2B), which may facilitate more protection comparatively. But on increasing the UV-C

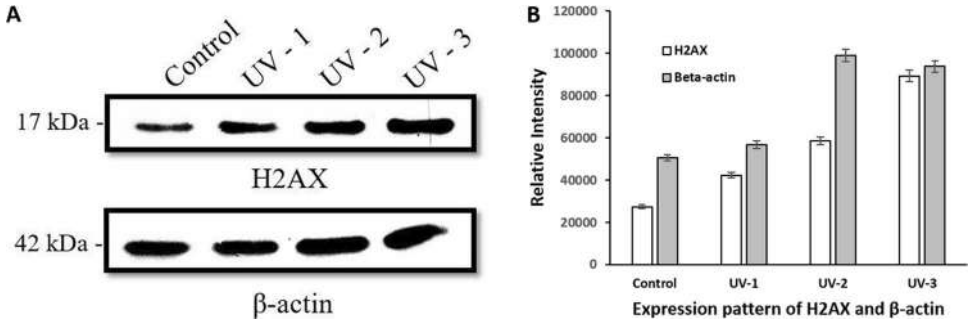

Figure 8. H2AX and β-actin expression in the earthworm, *P. excavatus* after 20 h of post UV-C exposure—(**A**) Western blot analysis, H2AX expression is gradually increased in 1 and 2 min UV-C exposed earthworms; in 3 min UV-C-treated group double the expression of H2AX was observed when compared with the control group. Similarly, β-actin, the reference protein also shows upregulated expression as the dose of UV-C increases. (**B**) Quantification of H2AX and β-actin expression are done based on the band intensity and represented using bar diagram. To analyse the statistical significance, the experiments were repeated in triplicate and their value is represented as mean ± SD. p-value < 0.05 was considered as a statistically significant data.

exposure time (5 min), the nature of the exorcizing coelomic fluid changes results in secreting flimsy, colorless coelomic fluid (Fig. 2C), which appears as white color patches on the dorsal surface following 15 h of post UV-C treatment (Fig. 2D–F) is noted. The secretion of coelomic fluid is protective to certain extent but increasing the UV-C dose is not able to protect their skin from burn and subsequent death occurs. In human and some animals following UV irradiation, high amount of mediators is released through the skin, which include eicosanoids (PGE2, PGD2, PGF2a, LTB-4, 12-HETE), cytokines (IL-1, IL-6, IL-8, TNF-alpha), growth factors (TGF-beta, VEGF, NGF), vasoactive amines, and neuropeptides (histamine, bradykinin, CGRP)[33]. Some report suggesting that some chemicals and enzymes protect the organism from UV radiations; such as mycosporine-like amino acid and flavonol quercetin or photolyase[34–36].

Following exposure to UV-C, the ventral side of earthworm becomes slight yellowish when compared to control worms (Fig. 4C,F,I,L,O). It can be due to the increase in production of coelomic fluid and their stagnation at the site of damages. In earthworm, respiration is depending on the network of small blood vessels present in the body wall epidermis. The oxygen is taken from the moist surface of the body wall, which keeps moisture by mucous gland of the epidermis[28]. When exposed to increased dose of UV-C, the epidermis and mucous gland get damaged, which makes it difficult to respire and leads to suffocation. Likewise, coelomic fluid circulation mainly depends on muscle contraction and the damaged epithelium causes abnormal muscle contraction that also leads to suffocation[37]. While exposing to UV-C, we observe the vigorous behavior of earthworm and the worm tries to avoid the UV exposure, possibly due to the effect on sensory neurons. Similarly, zebrafish larvae also have negative phototaxis when exposed to UV light[38]. In the earthworm body, there are nerve fibers and nerve plexus (motor neuron and sensory neuron), which arise from the segmental neuron. Specifically, nerve plexus occurs in the epidermis and it is well observed that the sensory cell of the epidermis transmits impulses directly to muscles as well as to the central nervous system of earthworm[39]. Hence, UV-C radiation effects on motor neuron leads to muscle constrain. In the meantime, muscular coordination between the circular and longitudinal layer is very essential for proper muscular contraction[37] and in UV-C-exposed worms, the circular and longitudinal layers are damaged, which directly affects the crawling of earthworm. Collectively, upon increasing UV-C dose, the amount of coelomic fluid released is gradually increased and at the same time tissue respiration is highly affected.

Tissue response and assessment of autotomy. Many studies report the effects of UV radiation on several organisms[40–42]. In particular on earthworm, Chuang et al. in 2006 reported that the earthworm, *Amynthas gracilis* tolerate UV-A, dies when exposed to UV-B, and shows lower tolerance than *Metaphire posthuma* species when exposed to UV-B. But *Pontoscolex corethrurus* species show the highest tolerance and survival ability even at a high dose of UV-B[37]. In our present study, *P. excavatus* survive up to 15 h of post-UV-C treatment in all groups, but after 20 h of post UV treatment, damages are visible, which is directly proportional to the exposure dose of UV-C. The formation of white patches on the dorsal surface of the skin following UV-C exposure are commonly observed in all groups, except in 1 min UV-C-treated earthworms. Similarly, the zebrafish produces a systemic anti-inflammatory and strong proinflammatory responses upon UV radiation[43]. However, the link between UV-B and immunity is reported in mice that UV-B suppresses the immune system by inhibiting memory and effector T-cells[44]. It also prevents atherosclerosis by regulating immuno-inflammatory reactions[45]. In earthworm, immune cells are loaded in the coelomic fluid and its increasing secretion following UV-C exposure definitely triggers inflammatory responses associated with damage of cells. However, the mechanism of earthworm immunity needs to be thoroughly studied.

Several reports have shown that UV induces production of reactive oxygen species, photo-oxidation, and increase in the oxidative damage to biomolecules[46–48]. Earthworm, *Lumbricus terrestris* secretes a photoreactive sterol and produces singlet following UV-A exposure[49]. Similarly, UV-A induces apoptosis in the central nervous system in a p53-dependent manner[50]. In our study, few worms in 3 min and most of the worms in 5 min

UV-treated groups showed knot-like structure formation (Fig. 4J,K,M,N) and it is referred to as inflammation. However, similar kinds of inflammation are not visible in the regions where most of the organs are present, which are located within 3rd to 18th segments which includes clitellum. The organs present in these segments may prevent them from visible UV damages than where no organ is present. There are multiple pathways for regulated cell death[51]. Still, UV-C induces death in earthworms and may perhaps lead by apoptosis and/or necrosis pathways. In Ly-5 murine lymphoma cells, UV-C induces apoptosis rather than necrosis[52]. Several organisms like amphibians, reptiles, fishes, and arthropods have a special kind of defence quality to escape from predators by a special process named autotomy[53].

Autotomy is also reported in earthworm, *Eudrilus eugeniae* in which it helps to eliminate toxic material from their body. Earthworm accumulates the toxic material at the most end segments of the tail region and detaches them to survive the remaining parts of the body[30]. In our study, the forming of cleavage furrow (Fig. 5C) proceeds further with a detachment of damaged segments (Figs. 4G,5D) and it happens mostly in the post clitellum region (Figs. 4G, 5C,D). Since the exposure of UV-C radiation on earthworm exposes all over the body and causes lethal effect, it is not possible to remove the genotoxic effects through autotomy process. In order to survive, worms can only stretch to detach the segments at the end of the tail region (Figs. 4G,5B); but even after a successful detachment, either part of the worm fails to stay alive, suggesting that earthworm can survive using autotomy against lower toxic chemicals not when completely exposed to genotoxic UV-C. However, its competence of autotomy on genotoxic needs to be evaluated by further pointed UV exposure studies.

Notably, we observe that whenever the dose of UV-C increases, the damage is deep and highly visible in their skin tissues. Moreover, we observed outgrowth of intestinal tissue structures, which narrow down the intestine and coelomic cavity free flow spaces in the dorsal side (highly exposed tissue) and accumulate the coelomocytes towards damaged dorsal skin tissue (Fig. 6K,N). Similarly, in ventral side it was towards the intestinal tissue not towards the ventral skin. However, this accumulation of coelomocytes make way for free flow towards longitudinal layer tissue of the ventral side (Fig. 6L,O). In overall, overgrowth of chloragogen establishes increased production of coelomic fluid, these overproduction make more coelomocytes availability towards damaged tissue. Upon UV exposure, overproduction of coelomocytes is reported in sea urchin species[54] and also in response to wound, the accumulation of coelomocytes occurs near wound sites in earthworm species[55], which supports our findings. These efforts show that worms attempt to tackle the tissue damage made by the UV-C. In contrast, interestingly this accumulated pressure in the coelomic cavity and intestinal epithelium overgrowth influence to shut the intestinal food path (Fig. 6J,M). In *Metaphire posthuma*, following 36 h of post UV-B exposure, the epidermis is pleated, and some epidermal cells show necrosis. But after 48 h of post exposure, the epidermis is damaged and some circular muscles are deformed[37]. Notably, these effects are dependent on the dose and species tolerance, but in *P. excavatus* earthworm, it initiates deadly effect within a day. Based on our data, the effect of UV-C on earthworm shows obvious impacts and the phenotypical, pathological, and lethal assessment confirms that UV-C is more harmful radiation than any other subdivided UV spectrum.

The linkage between genome integrity and gene regulation. One of the main effects of radiation exposure is the formation of single strand (ssDNA) and DNA double-strand breaks (DSB) together referred to as DNA damage[56]. High DSB levels can lead to cell death and low levels of DSB result in genomic rearrangements and may lead to cancer. In this present study, DNA fragmentation assay shows a clear picture of DNA damage when earthworms are exposed to certain dose of UV-C (Fig. 7A). Many studies reveal that UV irradiation induces apoptosis[57,58] and few studies refer comet assay for indication of apoptosis[59] and some referred alkaline comet assay for single strand DNA break. We performed alkaline comet assay and it further confirms that UV-C induces significant damage to the earthworm DNA in a dose-dependent manner (Fig. 7B). Tissue size of about 10–12 segments is taken for the sample preparation, which include all the tissue layers from both dorsal and ventral side. Therefore, we observed different size of the comet tail structure. But the high number of comet tails are observed in 2 min- and 3 min-treated animals, whereas the long comet tails are observed in 3 min and 5 min-treated groups. However, 1 min-treated group also shows very few small comet tail DNA, which indicates that even in 1 min of UV exposure, it can damage the earthworm DNA and it could be in the outer layer tissue but it does not lead to death of the animal. The number of comet tail DNA in 5 min-treated group is lower than the 3 min-treated group. It might be due to DNA degradation and the DNA degradation during apoptosis is well discussed[60]. An author discusses the importance of DNA fragmentation in apoptosis and also suggests that during DNA fragmentation, DNA DSB can promote efficient apoptosis[61]. However, DNA degradation during UV-induced apoptosis in earthworms needs a detailed study. Through the tissue inflammation (Fig. 4J,K,M,N) and DNA damage (Fig. 7A,B), we infer that the UV-C-induced death in earthworm may be caused by both necrosis and apoptosis pathways.

During apoptosis, the initial DNA fragmentation encourages H2AX phosphorylation[62]. Many reports support the importance of the histone variant H2AX in various other biological processes including cell division, embryonic development, neural stem cell development, and ageing[63]. Mainly H2AX phosphorylation is considered in response to the DNA DSB and ssDNA formation. However, the UV-C that we used in this experiment does not produce DSB directly, but produces cyclobutane pyrimidine dimers (CPDs) and 6–4 photoproducts (6-4PP) majorly[64]. Several reports suggest that H2AX phosphorylation depends on nucleotide excision repair (NER)[65,66]. In addition, UV radiation also generates DSB in an NER-dependent manner[56] and unrepaired SSB develops into DNA DSB during mitosis[67] The H2AX phosphorylation in response to DSB formation mediated by the major physiological factor ATM kinase[68] but for ssDNA formation ATR (the ATM- and Rad3-related protein kinase) phosphorylates the H2AX[69]. But, phosphorylation of H2AX is mediated by all phosphoinositide 3-kinase-related protein kinases (PIKKs), ATM, ATR, and DNA-dependent protein kinase (DNA-PK) in the case of DNA damage caused by radiation[70] suggesting that radiation causes ssDNA formation and DNA DSB.

Although H2AX is largely considered to be a DNA damage marker, UV irradiation induces phosphorylation of H2AX[71]. In human cell lines, γH2AX formation is gradually increased up to 4 h when irradiated with 10–40 J/m^2 of UV-C[72]. Our result confirms that upregulation of H2AX is directly proportional to the increased level of DNA damages. The combined evidence suggests that DNA fragmentation or damage induced through UV-C radiation causes ssDNA formation and DSB, which leads to apoptosis and phosphorylation of H2AX as the signal for initiation of counteraction. However, increased dose of UV-C associated with increased DNA damage and apoptosis leads to mortality in earthworm.

Several attempts have been made in the past to identify stable and convenient endogenous control genes in human studies. Reports suggest that UV-B irradiation in human skin fibroblasts, β-actin and TUBB1 are used as the reference genes[73]. Hence, we use β-actin as a reference gene for our experiments. Interestingly, we note β-actin gene expression is upregulated and it is visible in 2 min- and 3 min-treated groups (Fig. 8) when compared to control. Many of the reports show that the commonly used reference genes are not stable, the low-dose X-ray irradiation downregulates β-actin[74]; unregulated CDKN1A[75];18S and B2M genes are unstable under different radiation in human cells[76]. In addition, recent studies show that one of the prominent reference gene, GAPDH expression significantly vary in the earthworm, *Eisenia fetida* under the exposure of UV filter 4-Hydroxybenzophenone[77]. Therefore, housekeeping genes stability varies depending on cellular pathway response to the toxin. From our results, the upregulated expression of β-actin may be due to the need of the cells to maintain the cellular integrity following UV-C exposure.

Conclusion

Based on behavioral, phenotypical, pathological, lethal effect, DNA damage, and the expression of H2AX analyzed in our study, we conclude that the earthworm, *P. excavatus* is highly sensitive to UV-C. Notably, frequency of those changes increases in the earthworm with an enhanced dose of UV-C. Further, UV-C affects the earthworm system and generate the ssDNA and DNA double strand breaks, thereby disturbing the genome integrity. Our study suggests that UV-C-induced cell death in earthworm is lead by apoptosis and necrosis pathway. Moreover, this study confirms the presence of H2AX protein in earthworm, which shows DNA damage response similar to higher animals like vertebrates. Since earthworms are widely used as an animal model system for regeneration and toxicology studies, our data steps the use of earthworm animal model in radiation research. In addition, we suggest that H2AX can be adopted as a marker for genotoxicity studies. On the other hand, we are focusing to study the influences of UV-C on earthworm regeneration.

Materials and methods

Earthworm culture. Earthworm, *P. excavatus* are purchased from 'Karthik Vermi-compost Industry, Vadipatti, Madurai, India'. Worms are cultured in a plastic container filled with fine soil, cow dung, and leaf litters. Jaggery filtrates are regularly sprayed to the soil for effective culturing of earthworms. The containers are maintained with moisture at ambient temperature around 20–25 °C in a good ventilated room. The worm bed is regularly changed once every month by removing the vermicompost and compensates with soil and leaf litters.

Ethical statement. The experiments are carried out using lower invertebrate, earthworm therefore ethical statement is not needed. Necessary care is taken in experimental procedure that are intended to avoid unnecessary pain and suffering to the experimental animals.

UV-C treatment. The mature worms weighing around 300 mg are selected for the present experimental studies. The worms are divided into five experimental groups and each group has ten worms in total. All the group worms are taken in a separate (20 × 18 × 15 cm) plastic tray. To maintain the wet surface, 10 ml of water is filled into the tray so that the tray is wet for few minutes. Following that, the worms are exposed to UV-C for different time periods 1, 2, 3, and 5 min. The UV source is laminar airflow and wavelength of that UV-C light is 253.7 nm and the exposed area is 120 × 60 × 55 cm. Consequently, exposure dose is calculated as 1 min = 1.423×10^{-17} J/m^2, 2 min = 2.85×10^{-17} J/m^2, 3 min = 4.27×10^{-17} J/m^2, 5 min = 7.13×10^{-17} J/m^2 (detailed calculation available in supplementary data 1). But the control groups are not exposed to the UV-C. Following one-time UV-C exposure, all the worms are maintained in a regular bed. After 15th and 20th hours of post UV treatment, the visible physiological changes are analyzed. All the samples are collected from the post clitellum region of earthworm for following experiments.

Histology. Histology is performed to study the impact of UV-C-treated earthworms by analyzing the cellular structures, morphological changes, and tissue damage. Briefly, worm tissues are fixed with 10% formalin for 24 h. Then gradient (60–100%) isopropyl alcohol is used to dehydrate followed by clearing it with xylene. Following the clearing step, the tissue samples are embedded with paraffin wax. The embedded tissues are sectioned into 6 µm thick sections using a rotary microtome (Leica-RM2125 RTS). Further, the sections are rehydrated and stained with Hematoxylin and Eosin mounted with DPX mounting agent. The results are observed under light microscope (Leica-DM2000LED) and documented.

DNA extraction and DNA fragmentation assay by agarose gel electrophoresis. DNA is isolated from all the earthworm groups, including control worms, UV-C 1, 2, 3, and 5 min-treated groups. In brief, the small pieces of tissues are taken and washed with ice-cold PBS buffer. Then it is taken in the vial and added with 50 µl of digestion buffer, homogenized and further incubated at 50 °C for 6–12 h. Following incubation, homogenized tissues are added with equal amount of a mixture of phenol, chloroform, and isopropyl alcohol in the

ratio of (25:24:1) and kept in a rocker for 10 min. At that point, transfer the aqueous layer to a fresh tube and add half the volume of ammonium acetate and double the volume of 100% ethanol. Later, centrifuge this mixture at 10,000 rpm for 2 min. Subsequently, remove the supernatant and add 700 µl of 70% ethanol to the pellet and mix well. Repeat the step again and dry the pellet for a few minutes. Finally, add 50 µl of 1 × TE buffer to the dried pelleted DNA, mix well, and store it at 4 °C. The isolated DNA is in 1% agarose gel electrophoresis. DNA bands are analyzed and compared with the control group.

Comet assay. *Cell isolation.* The earthworm tissue is washed with ice cold water and cut into very small tissue fragments. Then the cell is dissociated from the tissue fragment in ice cold PBS containing 50 mM EDTA and 0.1% trypsin by using fine needles. Further, transfer the cell suspension into a centrifuge tube and allow to stand it for 5 min at room temperature to settle down the debris. Subsequently, the supernatant is collected by centrifugation at 1000 rpm for 4 min, the supernatant is discarded and the pellet is added with ice cold PBS. Repeat the step once again and collect the cell and mix it well with ice cold PBS and keep at 4 °C in dark condition.

Slide preparation. The Comet slide base layer is coated with the 0.75% low melting agarose on frosted glass slide at a temperature of 40 °C. Then it is kept at 4 °C for 15 min. Later, the earthworm cell suspension is mixed with low melting agarose in 1:10 ratio at 37 °C. Subsequently, 100 µl of this suspension is taken and coated on the base layer of the prepared slide and allowed to dry at 4 °C for 15 min in dark condition.

Further, it is treated with lysis buffer (contains triton × 100) for 1 h followed by incubation in alkaline solution for 30 min in ice cold condition. Then it is run in the electrophoresis at 35 V for 15 min. Later slides are transferred into pre-chilled water and immersed for 2 min twice. Later, transfer it to pre-chilled 70% ethanol for 5 min and allow it to dry in a horizontal position. Finally, the slides are incubated with Bisbenzimide Hoechst 3342 fluorescent stain for 15 min followed by documentation using Evos inverted fluorescence microscope.

SDS PAGE and immunoblotting. The earthworm, *P. excavatus* tissues are taken for the protein sample preparation. Briefly, tissues are homogenized with 2 × protein sample buffer and the homogenate are boiled for 5 min. Subsequently, 10 µg of each protein samples are resolved in 12% SDS-PAGE. The resolved proteins in the SDS-PAGE gel are transferred to the PVDF membrane. The membrane is then incubated with a primary antibody, H2AX (Rabbit polyclonal, Abcam-ab20669), and β-Actin (Mouse monoclonal, Abcam-ab8227) at the dilution of 1:5000 at 4 °C for 6 h. Following incubation, the membrane is washed with 1 × PBST buffer thrice and incubated with secondary antibody, anti-rabbit IgG, HRP (produced in goat, Sigma-A0545), and Anti-mouse IgG, HRP (produced in goat Abcam-ab6789) at a dilution of 1:10,000 for 2 h at room temperature. Following the washing step, the band signals in the membrane are developed using an X-ray film. The ECL is a chemiluminescent substrate used for the detection of horseradish peroxidase (HRP). After incubating the membrane in ECL substrate solution for 1 min, the membrane is removed and excess liquid is drained out. Then the membrane is placed inside the transparent plastic sheet and positioned inside the cassette followed by situating an X-ray film over it to close the cassette to capture the signals. After 5 min of exposure, the X-ray film is immersed few times in the developer solution and the signals in the X-ray film are developed followed by immersion in water. Later, immerse it in fixture solution followed by water. Then, the X-ray film is allowed to dry for documentation.

Statistical analysis. Survival graph (Kaplan–Meier) for the UV-C-treated earthworms is plotted using the statistical software—GraphPad Prism, Version 5.01. Briefly, UV-C treatment of the earthworms, death, and live worms are counted and plotted in the (Kaplan–Meier) survival graph. All other experiments are repeated for at least three times to obtain the statistical significance. The data obtained were analysed using the statistical software SPSS (version 22.0; IBM Corp., USA) and expressed as mean ± SD. The results were considered as statistical significance when the p-value < 0.05.

Data availability

All data generated or analyzed during this study are included in this published article.

Received: 1 November 2019; Accepted: 17 November 2020
Published online: 03 December 2020

References

1. Hoeijmakers, J. H. J. DNA damage, aging, and cancer. *N. Engl. J. Med.* **361**, 1475–1485 (2009).
2. Roy, S., Choudhury, S. R., Singh, S. K. & Das, K. P. AtPolλ, a homolog of mammalian DNA polymerase λ in Arabidopsis thaliana, is involved in the repair of UV-B induced DNA damage through the dark repair pathway. *Plant Cell Physiol.* **52**, 448–467 (2011).
3. MacRae, S. L. *et al.* DNA repair in species with extreme lifespan differences. *Aging (Albany, NY)* **7**, 1171 (2015).
4. Gartner, A., Milstein, S., Ahmed, S., Hodgkin, J. & Hengartner, M. O. A conserved checkpoint pathway mediates DNA damage-induced apoptosis and cell cycle arrest in *C. elegans*. *Mol. Cell* **5**, 435–443 (2000).
5. O'Driscoll, M. & Jeggo, P. A. The role of double-strand break repair—insights from human genetics. *Nat. Rev. Genet.* **7**, 45 (2006).
6. Stucki, M. & Jackson, S. P. γH2AX and MDC1: anchoring the DNA-damage-response machinery to broken chromosomes. *DNA Repair (Amst)* **5**, 534–543 (2006).
7. Thiriet, C. & Hayes, J. J. Chromatin in need of a fix: phosphorylation of H2AX connects chromatin to DNA repair. *Mol. Cell* **18**, 617–622 (2005).
8. Nussenzweig, A. & Paull, T. DNA repair: tails of histones lost. *Nature* **439**, 406 (2006).
9. Ünal, E. *et al.* DNA damage response pathway uses histone modification to assemble a double-strand break-specific cohesin domain. *Mol. Cell* **16**, 991–1002 (2004).
10. Sinha, R. P. & Häder, D.-P. UV-induced DNA damage and repair: a review. *Photochem. Photobiol. Sci.* **1**, 225–236 (2002).

11. Guerrero-Beltr-n, J. A. & Barbosa-C· novas, G. V. Advantages and limitations on processing foods by UV light. *Food Sci. Technol. Int.* **10**, 137–147 (2004).
12. Steeger, H.-U., Freitag, J. F., Michl, S., Wiemer, M. & Paul, R. J. Effects of UV-B radiation on embryonic, larval and juvenile stages of North Sea plaice (*Pleuronectes platessa*) under simulated ozone-hole conditions. *Helgol. Mar. Res.* **55**, 56 (2001).
13. Misra, R. B., Babu, G. S., Ray, R. S. & Hans, R. K. Tubifex: a sensitive model for UV-B-induced phototoxicity. *Ecotoxicol. Environ. Saf.* **52**, 288–295 (2002).
14. Bais, A. F. *et al.* Environmental effects of ozone depletion, UV radiation and interactions with climate change: UNEP Environmental Effects Assessment Panel, update 2017. *Photochem. Photobiol. Sci.* **17**, 127–179 (2018).
15. Dixon, A. J. & Dixon, B. F. Ultraviolet radiation from welding and possible risk of skin and ocular malignancy. *Med. J. Aust.* **181**, 155–157 (2004).
16. Welch, D. *et al.* Far-UVC light: A new tool to control the spread of airborne-mediated microbial diseases. *Sci. Rep.* **8**, 2752 (2018).
17. Wu, J. *et al.* The influence of postharvest UV-C treatment on anthocyanin biosynthesis in fresh-cut red cabbage. *Sci. Rep.* **7**(1), 5232 (2017).
18. Bintsis, T., Litopoulou-Tzanetaki, E. & Robinson, R. K. Existing and potential applications of ultraviolet light in the food industry—a critical review. *J. Sci. Food Agric.* **80**, 637–645 (2000).
19. Manuela, B., Welch, D., Igor, S. & Brenner, D. J. Far-UVC light (222 nm) efficiently and safely inactivates airborne human coronaviruses. *Sci. Rep.* **10**(1), 10285 (2020).
20. Pourzand, C. & Tyrrell, R. M. Apoptosis, the role of oxidative stress and the example of solar UV radiation. *Photochem. Photobiol.* **70**, 380–390 (1999).
21. Davies, R. J. H. Ultraviolet radiation damage in DNA. *Biochem. Soc. Trans.* **23**, 407–418 (1995).
22. Fernandez-Capetillo, O., Lee, A., Nussenzweig, M. & Nussenzweig, A. H2AX: the histone guardian of the genome. *DNA Repair (Amst).* **3**, 959–967 (2004).
23. Celeste, A. *et al.* Genomic instability in mice lacking histone H2AX. *Science* **296**, 922–927 (2002).
24. Pilch, D. R. *et al.* Characteristics of γ-H2AX foci at DNA double-strand breaks sites. *Biochem. Cell Biol.* **81**, 123–129 (2003).
25. Hanasoge, S. & Ljungman, M. H2AX phosphorylation after UV irradiation is triggered by DNA repair intermediates and is mediated by the ATR kinase. *Carcinogenesis* **28**, 2298–2304 (2007).
26. Diffey, B. L. Solar ultraviolet radiation effects on biological systems. *Phys. Med. Biol.* **36**, 299 (1991).
27. Modenese, A., Korpinen, L. & Gobba, F. Solar radiation exposure and outdoor work: an underestimated occupational risk. *Int. J. Environ. Res. Public Health.* **15**, 2063 (2018).
28. Edwards, C. A. & Bohlen, P. J. *Biology and ecology of earthworms* 3rd edn. (Springer Science & Business Media, New York, 1996).
29. Johnson Retnaraj Samuel, S. C. *et al.* Autofluorescence in BrdU-positive cells and augmentation of regeneration kinetics by riboflavin. *Stem Cells Dev.* **21**, 2071–2083 (2011).
30. Yesudhason, B. V. *et al.* Exploiting the unique phenotypes of the earthworm *Eudrilus eugeniae* to evaluate the toxicity of chemical substances. *Environ. Monit. Assess.* **190**, 145 (2018).
31. Engelmann, P., Pál, J., Berki, T., Cooper, E. L. & Németh, P. Earthworm leukocytes react with different mammalian antigen-specific monoclonal antibodies. *Zoology* **105**, 257–265 (2002).
32. Płytycz, B., Homa, J., Kozioł, B., Rózanowska, M. & Morgan, A. J. Riboflavin content in autofluorescent earthworm coelomocytes is species-specific. *Folia Histochem. Cytobiol.* **44**(4), 275–280 (2006).
33. Clydesdale, G. J., Dandie, G. W. & Muller, H. K. Ultraviolet light induced injury: immunological and inflammatory effects. *Immunol. Cell Biol.* **79**, 547–568 (2001).
34. Banaszak, A. T. & Trench, R. K. Effects of ultraviolet (UV) radiation on marine microalgal-invertebrate symbioses. II. The synthesis of mycosporine-like amino acids in response to exposure to UV in *Anthopleura elegantissima* and *Cassiopeia xamachana*. *J. Exp. Mar. Biol. Ecol.* **194**, 233–250 (1995).
35. Carefoot, T. H., Harris, M., Taylor, B. E., Donovan, D. & Karentz, D. Mycosporine-like amino acids: possible UV protection in eggs of the sea hare *Aplysia dactylomela*. *Mar. Biol.* **130**, 389–396 (1998).
36. Inal, M. E. & Kahraman, A. The protective effect of flavonol quercetin against ultraviolet a induced oxidative stress in rats. *Toxicology* **154**, 21–29 (2000).
37. Chuang, S.-C., Lai, W.-S. & Chen, J.-H. Influence of ultraviolet radiation on selected physiological responses of earthworms. *J. Exp. Biol.* **209**, 4304–4312 (2006).
38. Guggiana-Nilo, D. A. & Engert, F. Properties of the visible light phototaxis and UV avoidance behaviors in the larval zebrafish. *Front. Behav. Neurosci.* **10**, 160 (2016).
39. Hess, W. N. Nervous system of the earthworm, *Lumbricus terrestris* L. *J. Morphol.* **40**, 235–259 (1925).
40. Holm-Hansen, O., Lubin, D. & Helbling, E. W. Ultraviolet radiation and its effects on organisms in aquatic environments. In *Environmental UV photobiology* 379–425 (Springer, 1993).
41. Soni, A. K. & Joshi, P. C. High sensitivity of Tubifex for ultraviolet-B. *Biochem. Biophys. Res. Commun.* **231**, 818–819 (1997).
42. van de Mortel, T. F. & Buttemer, W. A. Avoidance of ultraviolet-B radiation in frogs and tadpoles of the species *Litoria aurea*, *L. dentata* and *L, peronii*. *Proc. Linn. Soc. New South Wales* **119**, 173–179 (1998).
43. Banerjee, S. & Leptin, M. Systemic response to ultraviolet radiation involves induction of leukocytic IL-1β and inflammation in zebrafish. *J. Immunol.* **193**(3), 1408–1415 (2014).
44. Rana, S., Byrne, S. N., MacDonald, L. J., Chan, C.Y.-Y. & Halliday, G. M. Ultraviolet B suppresses immunity by inhibiting effector and memory T cells. *Am. J. Pathol.* **172**, 993–1004 (2008).
45. Sasaki, N. *et al.* UVB exposure prevents atherosclerosis by regulating immunoinflammatory responses. *Arterioscler. Thromb. Vasc. Biol.* **37**, 66–74 (2017).
46. Lesser, M. P., Farrell, J. H. & Walker, C. W. Oxidative stress, DNA damage and p53 expression in the larvae of Atlantic cod (*Gadus morhua*) exposed to ultraviolet (290–400 nm) radiation. *J. Exp. Biol.* **204**, 157–164 (2001).
47. Singh, M. K., Sharma, J. G. & Chakrabarti, R. Simulation study of natural UV-B radiation on *Catlacatla* and its impact on physiology, oxidative stress, Hsp 70 and DNA fragmentation. *J. Photochem. Photobiol. B Biol.* **149**, 156–163 (2015).
48. Ramírez-Duarte, W. F., Kurobe, T. & Teh, S. J. Effects of low levels of ultraviolet radiation on antioxidant mechanisms of Japanese Medaka (*Oryziaslatipes*). *Chemosphere* **181**, 304–312 (2017).
49. Albro, P. W., Bilski, P., Corbett, J. T., Schroeder, J. L. & Chignell, C. F. Photochemical reactions and phototoxicity of sterols: novel self-perpetuating mechanism for lipid photooxidation. *Photochem. Photobiol.* **66**, 316–325 (1997).
50. Morita, A. & Krutmann, J. Ultraviolet A radiation-induced apoptosis. *Methods Enzymol.* **319**, 302–309 (2000).
51. Tang, D., Kang, R., Berghe, T. V., Vandenabeele, P. & Kroemer, G. The molecular machinery of regulated cell death. *Cell Res.* **29**(5), 347–364 (2019).
52. Godar, D. E. & Lucas, A. D. Spectral dependence of UV-induced immediate and delayed apoptosis: the role of membrane and DNA damage. *Photochem. Photobiol.* **62**, 108–113 (1995).
53. Maginnis, T. L. The costs of autotomy and regeneration in animals: a review and framework for future research. *Behav. Ecol.* **17**, 857–872 (2006).
54. Cooper, E. L. (ed.) *Advances in comparative immunology* (Springer, New York, 2018).
55. Rinkevich, B. & Müller, W. E. (eds) *Invertebrate immunology* (Springer Science & Business Media, New York, 2012).

56. Wakasugi, M. *et al.* Nucleotide excision repair-dependent DNA double-strand break formation and ATM signaling activation in mammalian quiescent cells. *J. Biol. Chem.* **289**(41), 28730–28737 (2014).
57. Azzouz, D., Khan, M. A., Sweezey, N. & Palaniyar, N. Two-in-one: UV radiation simultaneously induces apoptosis and NETosis. *Cell Death Discov.* **4**(1), 1–13 (2018).
58. Lee, C. H., Wu, S. B., Hong, C. H., Yu, H. S. & Wei, Y. H. Molecular mechanisms of UV-induced apoptosis and its effects on skin residential cells: the implication in UV-based phototherapy. *Int. J. Mol. Sci.* **14**(3), 6414–6435 (2013).
59. Araldi, R. P. *et al.* Using the comet and micronucleus assays for genotoxicity studies: a review. *Biomed. Pharmacother.* **72**, 74–82 (2015).
60. Nagata, S., Nagase, H., Kawane, K., Mukae, N. & Fukuyama, H. Degradation of chromosomal DNA during apoptosis. *Cell Death Differ.* **10**(1), 108–116 (2003).
61. Zhang, J. H. & Ming, X. U. DNA fragmentation in apoptosis. *Cell Res.* **10**(3), 205–211 (2000).
62. Rogakou, E. P., Nieves-Neira, W., Boon, C., Pommier, Y. & Bonner, W. M. Initiation of DNA fragmentation during apoptosis induces phosphorylation of H2AX histone at serine 139. *J. Biol. Chem.* **275**(13), 9390–9395 (2000).
63. Turinetto, V. & Giachino, C. Survey and summary multiple facets of histone variant H2AX: a DNA double-strand-break marker with several biological functions. *Nucleic Acids Res.* **43**, 2489–2498 (2015).
64. Friedberg, E. C. *et al.* (eds) *DNA repair and mutagenesis* (American Society for Microbiology Press, Washington, 2005).
65. Marti, T. M., Hefner, E., Feeney, L., Natale, V. & Cleaver, J. E. H2AX phosphorylation within the G1 phase after UV irradiation depends on nucleotide excision repair and not DNA double-strand breaks. *Proc. Natl. Acad. Sci. U.S.A.* **103**(26), 9891–9896 (2006).
66. O'Driscoll, M., Ruiz-Perez, V. L., Woods, C. G., Jeggo, P. A. & Goodship, J. A. A splicing mutation affecting expression of ataxia–telangiectasia and Rad3-related protein (ATR) results in Seckel syndrome. *Nat. Genet.* **33**(4), 497–501 (2003).
67. Caldecott, K. W. Single-strand break repair and genetic disease. *Nat. Rev. Genet.* **9**(8), 619–631 (2008).
68. Kastan, M. B. & Lim, D. S. The many substrates and functions of ATM. *Nat. Rev. Mol. Cell Biol.* **1**(3), 179–186 (2000).
69. Ward, I. M. & Chen, J. Histone H2AX is phosphorylated in an ATR-dependent manner in response to replicational stress. *J. Biol. Chem.* **276**(51), 47759–47762 (2001).
70. Wang, H., Wang, M., Wang, H., Böcker, W. & Iliakis, G. Complex H2AX phosphorylation patterns by multiple kinases including ATM and DNA-PK in human cells exposed to ionizing radiation and treated with kinase inhibitors. *J. Cell. Physiol.* **202**(2), 492–502 (2005).
71. Oh, K.-S., Bustin, M., Mazur, S. J., Appella, E. & Kraemer, K. H. UV-induced histone H2AX phosphorylation and DNA damage related proteins accumulate and persist in nucleotide excision repair-deficient XP-B cells. *DNA Repair (Amst).* **10**, 5–15 (2011).
72. Wakasugi, M. *et al.* Nucleotide excision repair-dependent DNA double-strand break formation and ATM signaling activation in mammalian quiescent cells. *J. Biol. Chem.* **289**, 28730–28737 (2014).
73. Li, L., Yan, Y., Xu, H., Qu, T. & Wang, B. Selection of reference genes for gene expression studies in ultraviolet B-irradiated human skin fibroblasts using quantitative real-time PCR. *BMC Mol. Biol.* **12**, 8 (2011).
74. Miller, A. C. *et al.* Proto-oncogene expression: a predictive assay for radiation biodosimetry applications. *Radiat. Prot. Dosim.* **99**, 295–302 (2002).
75. Amundson, S. A. *et al.* Human in vivo radiation-induced biomarkers: gene expression changes in radiotherapy patients. *Cancer Res.* **64**, 6368–6371 (2004).
76. Sharungbam, G. D. *et al.* Identification of stable endogenous control genes for transcriptional profiling of photon, proton and carbon-ion irradiated cells. *Radiat. Oncol.* **7**, 70 (2012).
77. Novo, M., Muñiz-González, A. B., Trigo, D., Casquero, S. & Guitarte, J. L. M. Applying sunscreens on earthworms: Molecular response of *Eisenia fetida* after direct contact with an organic UV filter. *Sci. Total Environ.* **676**, 97–104 (2019).

Acknowledgements

Authors thank 'International Research Centre (IRC) of Sathyabama Institute of Science and Technology, Chennai' for proving all support to carry out the research work. In addition, authors thank the funding agency 'Department of Science and Technology – Science and Engineering Research Board (DST-SERB, Ref. No. ECR/2016/000956), New Delhi, India' for providing funding support.

Author contributions

S.C.K.—investigation, data curation, formal analysis, methodology, validation, writing-original draft; S.J.D.—conceptualization, project administration, resources, methodology, supervision, software, validation, writing-review and editing; A.A.—visualization; P.V.D.—visualization, formal analysis; J.M.—formal analysis, data curation; Y.B.V.—formal analysis, validation; C.V.N.—Methodology, data curation, formal analysis; G.M.—formal analysis, validation; R.K.—formal analysis, validation; V.S.—investigation, formal analysis; B.J.—formal analysis, validation; J.J.K.—formal analysis; S.J.R.S.—conceptualization, project administration, resources, methodology, supervision, software, validation, writing-review and editing and all the author reviewed the manuscript.

Competing interests

The authors declare no competing interests.

Additional information

Supplementary information is available for this paper at https://doi.org/10.1038/s41598-020-77719-2.

Correspondence and requests for materials should be addressed to J.D.S.C. or J.R.S.S.C.

Reprints and permissions information is available at www.nature.com/reprints.

Publisher's note Springer Nature remains neutral with regard to jurisdictional claims in published maps and institutional affiliations.

Open Access This article is licensed under a Creative Commons Attribution 4.0 International License, which permits use, sharing, adaptation, distribution and reproduction in any medium or format, as long as you give appropriate credit to the original author(s) and the source, provide a link to the Creative Commons licence, and indicate if changes were made. The images or other third party material in this article are included in the article's Creative Commons licence, unless indicated otherwise in a credit line to the material. If material is not included in the article's Creative Commons licence and your intended use is not permitted by statutory regulation or exceeds the permitted use, you will need to obtain permission directly from the copyright holder. To view a copy of this licence, visit http://creativecommons.org/licenses/by/4.0/.

© The Author(s) 2021

Summary of Research Excellence for Sun Pharma Research Fellowship

1. Multi-Functional Role of TCTP in Earthworm Regeneration

- **Publication:** Rajagopalan et al., *Tissue Engineering and Regenerative Medicine* (2024)
- **Key Contribution:** This study elucidates the role of Tumor Protein p53 (TCTP) in the regeneration of the earthworm *Perionyx excavatus*. It reveals how TCTP influences multiple aspects of tissue regeneration, highlighting its potential as a target for regenerative therapies.

  Rajagopalan, Kamarajan, **Jackson Durairaj Selvan Christyraj**, Karthikeyan Subbiahanadar Chelladurai, Puja Das, Karthikeyan Mahendran, Logeshwari Nagarajan, and Saritha Gunalan. "Understanding the multi-functional role of TCTP in the regeneration process of Earthworm, Perionyx excavatus." *Tissue Engineering and Regenerative Medicine* 21, no. 2 (2024): 353-366.

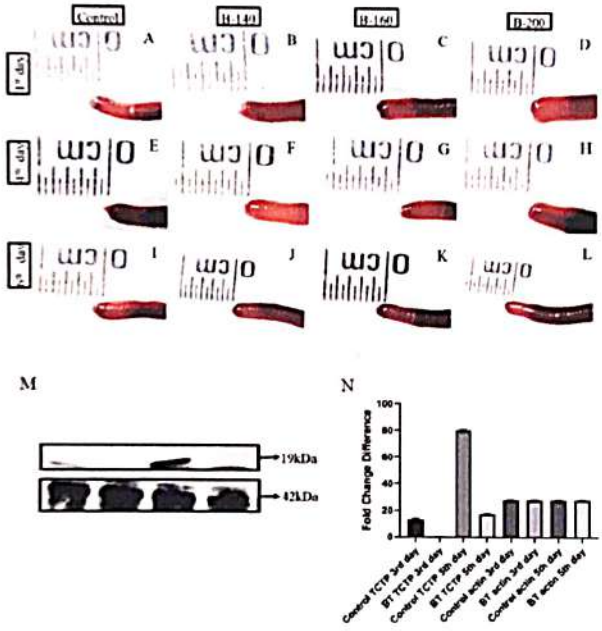

Figure 1 Pharmacological suppression of TCTP using buclizine and its effects on regeneration: A–D represents control worm (1X PBS), 140 lg buclizine, 160 lg buclizine, and 200 lg buclizine injected worms respectively following day-1 of post-amputation. E–H represents the 4th day post amputated worms correspondingly from the control worm (1X PBS), 140 lg buclizine, 160 lg buclizine, and 200 lg buclizine injected worms. In all the buclizineinjected worms, the regenerative bud size is hindered. Similarly, I-L represents the 6th day regenerative bud from the control worm, 140 lg buclizine, 160 lg buclizine, and 200 lg buclizine-injected worms, respectively. In all the buclizine-injected worms, regeneration is 1/4th reduced. M. Western blotting image represents TCTP (19 kDa) and b-actin (42 kDa) expression in 3rd day control regenerating worm, 3rd day buclizine injected regenerating worm, 5th day control

S. Jackson Durairaj
Dr. **S. Jackson Durairaj** PhD., NET,
Scientist-D/Associate Professor (Research),
Centre for Molecular and Nanomedical Sciences,
International Research Centre,
Sathyabama Institute of Science and Technology,
Jeppiaar Nagar, Rajiv Gandhi Salai, Chennai - 600 119,
Tamil Nadu, India.

regenerating worm and in 5th day buclizine injected regenerating worms respectively. N. graphical representation of Western blotting results shows the fold difference of TCTP and the expression of b-actin in control regenerating worms and the 5th day buclizine injected regenerating worms.

2. Impact of UV-C Radiation on Genomic Integrity

- **Publication:** Subbiahanadar Chelladurai et al., *Scientific Reports* (2020)
- **Key Contribution:** This research explores the effects of UV-C radiation on earthworm DNA, focusing on H2AX expression. It provides insights into how UV-C impacts genomic integrity and cellular repair mechanisms, enhancing understanding of environmental stress on cellular systems.

  Subbiahanadar Chelladurai, Karthikeyan, **Jackson Durairaj** Selvan Christyraj, Ananthaselvam Azhagesan, Vennila Devi Paulraj, Muralidharan Jothimani, Beryl Vedha Yesudhason, Niranjan Chellathurai Vasantha et al. "Exploring the effect of UV-C radiation on earthworm and understanding its genomic integrity in the context of H2AX expression." *Scientific Reports* 10, no. 1 (2020): 21005.

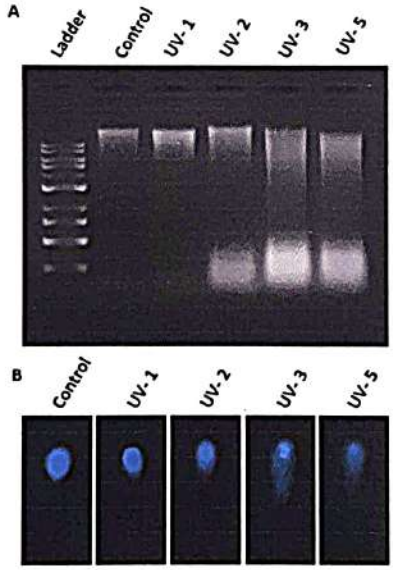

Figure 2. DNA fragmentation assay and Comet Assay. (A) DNA fragmentation assay—ladder (1 kb), Control group DNA with a single clear band and from 1, 2, 3, and 5 min UV-C-exposed earthworms, DNA are fragmented and come with dragged structure. Te DNA fragmentation dragged is high in UV-C 3 and 5 mintreated groups. (B) Comet assay—in control group, the DNA appears in a proper round structure whereas in 1–5 min UV-C-treated group, it shows increased tail movement.

S. Jackson Durairaj
Dr. **S. Jackson Durairaj** PhD., NET,
Scientist-D/Associate Professor (Research),
Centre for Molecular and Nanomedical Sciences,
International Research Centre,
Sathyabama Institute of Science and Technology,
Jeppiaar Nagar, Rajiv Gandhi Salai, Chennai - 600 119,
Tamil Nadu, India.